Large impact of extreme precipitation on projected blue–green water ~~shares~~partitioning

Simon P. Heselschwerdt[1,2], Thorsten Wagener[2], Lan Wang-Erlandsson[3,4,5,6], Anna M. Ukkola[7,8], Yannis Markonis[9], Yuting Yang[10,11], and Peter Greve[1]

[1]Climate Service Center Germany (GERICS), Helmholtz-Zentrum Hereon, Hamburg, Germany
[2]Institute of Environmental Science and Geography, University of Potsdam, Potsdam, Germany
[3]Stockholm Resilience Centre, Stockholm University, Stockholm, Sweden
[4]Bolin Centre for Climate Research, Stockholm University, Stockholm, Sweden
[5]Anthropocene Laboratory, The Royal Swedish Academy of Sciences, Stockholm, Sweden
[6]Potsdam Institute for Climate Impact Research (PIK), Member of the Leibniz Association, Potsdam, Germany
[7]ARC Centre of Excellence for Climate Extremes, University of New South Wales, Sydney, NSW, Australia
[8]Climate Change Research Centre, University of New South Wales, Sydney, NSW, Australia
[9]Department of Water Resources and Environmental Modeling, Faculty of Environmental Sciences, Czech University of Life Sciences Prague, Praha - Suchdol, Czech Republic
[10]State Key Laboratory of Hydroscience and Engineering, Department of Hydraulic Engineering, Tsinghua University, Beijing, China
[11]Key Laboratory of Hydrosphere Sciences of the Ministry of Water Resources, Beijing, China

Correspondence: Simon P. Heselschwerdt (simon.heselschwerdt@hereon.de)

Abstract. Precipitation partitioning into blue (runoff) and green water ~~resources (transpiration) flows~~ is a fundamental hydroecological process shaping freshwater availability across vegetated and hydrologically active land areas. This partitioning is determined by interactions among climatic conditions, land surface characteristics, and vegetation dynamics, which change with rising temperatures and CO_2 concentrations. Yet, future global shifts in ~~blue and green water shares and their management~~ blue–green water partitioning, their controlling factors, and their broader implications remain uncertain. We address this knowledge gap using ~~climate simulations to quantify~~ Earth system model simulations and define the Blue–Green Water Share (BGWS) metric to quantify changes in the relative partitioning of precipitation into ~~green and blue water flows and its controlling factors~~runoff and transpiration. Here, we show that increases in extreme five-day precipitation ~~primarily drives partitioning~~ are most strongly associated with future BGWS shifts, favouring larger blue water shares. This effect is independent of ~~baseline~~ mean precipitation increases and ~~generates larger blue water shares~~ occurs under both drying and wetting conditions. Additionally, ~~interactions between~~ increases in leaf area index ~~and plant water-use efficiency strongly impact regional partitioning trends~~tend to favour larger green water shares and counteract the blueward influence of stronger precipitation extremes. Our results ~~translate shifts in blue-green water partitioning into an impact-relevant perspective , providing actionable context for water and land management~~provide a process-based perspective on projected blue–green water partitioning and its hydroecological implications.

1 Introduction

Ongoing anthropogenic climate change and other human interventions ~~increasingly disrupt water availability and distribution. At the land surface, these disruptions interfere with precipitation partitioning, with profound implications for ecosystem functions and human water demands. Thus, understanding global~~ are reshaping the terrestrial water cycle and altering water availability globally (Wada et al., 2011; Greve et al., 2014; Milly and Dunne, 2016; Wada et al., 2016). These changes affect not only how much precipitation reaches the land surface, but also how that precipitation is partitioned among terrestrial water pathways. This matters because the same amount of precipitation can be divided into different shares of runoff, soil moisture, evaporation, and transpiration. This partitioning affects water availability in rivers, reservoirs, and aquifers, as well as ecosystems and land–atmosphere interactions (Falkenmark, 2013; Falkenmark et al., 2019; Gleeson et al., 2020a). Observations and Earth system models (ESMs) show that major land-water fluxes and stores are already changing in their amount, timing, and spatial distribution (Yang et al., 2023; Zaitchik et al., 2023; Gudmundsson et al., 2026). Understanding future water availability therefore requires understanding not only changes in precipitation ~~partitioning is critical for guiding sustainable water management~~itself, but also changes in how precipitation is partitioned at the land surface.

~~Addressing these challenges requires moving beyond the traditional blue water-centric perspective (Falkenmark and Rockström, 2010)~~To interpret precipitation partitioning in terms of its relevance for ecosystems and human water use, we use the blue–green water paradigm (Falkenmark, 1995; ~~. In this regard, Falkenmark (1995) advanced resource planning by incorporating the concept of green water and by later introducing the blue and green water paradigm~~ Falkenmark and Rockström, 2006). ~~Blue water encompasses aquifers, lakes, and reservoirsand sustains human activities such as~~ In this framework, blue water stores refer to water stored in lakes, reservoirs, and aquifers, while blue water flows include runoff; together, these stores and flows support drinking water supply, irrigation, ~~and industrial processes. It further stabilises Earth systems by supporting aquatic ecosystems and influencing the planet's energy balance (Wada et al., 2017; Falkenmark et al., 2019; Gleeson et al., 2020a)~~industrial use, and freshwater ecosystems (Falkenmark et al., 2019; Gleeson et al., 2020a). Green water ~~refers~~ stores refer to soil moisture in the unsaturated zone~~. It supports land system productivity and regulates critical processes such as carbon sequestration, climate regulation, and biodiversity maintenance. These two resources are governed by two complementary flows: green water flow, defined as transpiration , and blue water flow, involving water movement through, e.g., rivers or groundwater~~, which supports vegetation growth and terrestrial productivity and is returned to the atmosphere through green water flows, including transpiration and evaporation (Rockström and Gordon, 2001; Falkenmark et al., 2019; Gleeson et al., 2020a). Because blue and green water describe different forms and pathways of water availability, this framework complements standard variable-based hydrology by linking hydrological partitioning to its different roles for ecosystems and human water use.

We refer to the partitioning of precipitation into runoff and transpiration as blue–green water partitioning. Focusing on transpiration is useful because it captures a key pathway of plant water use, whereas metrics based on evapotranspiration (ET) or the complement of the runoff coefficient ($1 - RC$) describe broader water-loss or non-runoff signals and do not isolate vegetation-mediated water use (Lawrence et al., 2007; Denissen et al., 2022; Bouaziz et al., 2022). Better understanding how

precipitation is partitioned between runoff and transpiration is therefore important for interpreting shifts between runoff-related blue water availability and vegetation-mediated green water use.

~~Recent studies highlight that changes in green and blue water flows can compromise critical water functions, triggering both linear and non-linear responses within ecosystems and potentially crossing tipping points in the Earth system (Falkenmark et al., 2019; Gleeson et al., 2020a; Wang-Erlandsson et al., 2022). The resilience of the Earth system is already under threat, as green and blue water sub-boundaries have transgressed the global safe operating space defined by the planetary boundaries framework (Wang-Erlandsson et al., 2022; Richardson et al., 2023; Porkka et al., 2024; Rockström et al., 2024). Therefore, developing a comprehensive understanding of how climate change influences the global partitioning of precipitation into green and blue water flows is essential for safeguarding Earth system stability (Gleeson et al., 2020b)~~

~~Yet, complex responses to changing environmental conditions introduce uncertainty when projecting future pathways of blue-green water partitioning (Wei et al., 2025). This uncertainty is strongly linked to plants' twofold response to higher CO_2 concentrations. First, increased CO_2 levels enhance surface resistance to transpiration as plants close their stomata more frequently (Leakey et al., 2009). With all other parameters held constant, this may increase global streamflow (Idso and Brazel, 1984; Milly et al., 2005; Betts et al., 2007; Fowler et al., 2019). Similarly, higher~~ Under climate change, this blue–green water partitioning is expected to shift because the climatic and hydroecological controls on runoff and transpiration are changing at the same time. Rising CO_2 can reduce stomatal conductance and alter plant water-use efficiency (WUE)~~(the ratio of plant's carbon assimilation rate to transpiration rate) increases soil-moisture retention and reduces plant water stress (Swann et al., 2016). However, reduced transpiration also diminishes atmospheric moisture recycling, impacting local precipitation and regional-scale atmospheric circulation (Betts et al., 2004; Lee et al., 2012; Skinner et al., 2017). Second, elevated CO_2 levels promote the globally observed increase~~ , while changes in vegetation biomass ~~through CO_2 fertilisation, which can raise latent heat fluxes, enhance terrestrial water recycling, and amplify evaporative cooling and precipitation (Spracklen et al., 2012; Forzieri et al., 2020). Yet, the corresponding rise in freshwater demandsimultaneously reduces streamflow in some regions, exerting additional pressure on blue water availability (Ukkola et al., 2016; Mankin et al., 2017, 2018).~~

~~Besides plant CO_2 responses and other land surface processes, climatic factors and precipitation intensity strongly influence blue and green water flows (Trenberth, 1999; Gedney et al., 2014). Extreme precipitation events generate saturation and infiltration-excess runoff, largely depending on rainfall intensity~~ can modify terrestrial water use and runoff responses (Leakey et al., 2009; Swann et al., 2016; Ukkola et al., 2016; Zhu et al., 2016; Mankin et al., 2018) . At the same time, changes in atmospheric demand, ~~antecedent soil moisture,~~ soil moisture, and ~~soil infiltration capacity (Horton, 1933; Dunne and Black, 1970). As these events become more frequent under climate change, they are expected to increase~~ precipitation characteristics, including rainfall intensity and seasonality, can alter the balance between infiltration, storage, runoff generation, and transpiration ~~(Donat et al., 2016; Skinner et al., 2017; Yin et al., 2018; Tabari, 2020; Scheff et al., 2022). Future changes in blue–green water partitioning therefore reflect interacting changes in climate and vegetation rather than changes in precipitation alone.~~

A growing body of work has already examined related aspects of precipitation partitioning. Studies of drought and climate change show that runoff and ET or transpiration can respond differently, with blue water flows (Donat et al., 2016; Yin et al., 2018; Tabari, 2020). Consistently, offline Land Surface Model (LSM) experiments demonstrate that temporal concentration of precipitation is a first-order control on projected runoff ratios (Scheff et al., 2022).

Beyond changes in total blue and in some regions declining more strongly than green water flows , recent studies directly interrogate precipitation partitioning. Earth System Model (ESM) analyses show that increasing vegetation activity reduces runoff across about half (Ukkola et al., 2016; Orth and Destouni, 2018). ESM analyses further show that vegetation change can reduce runoff across large parts of vegetated land(Mankin et al., 2018). Particularly in the mid-latitudes, longer and warmer growing seasons reduce runoff even , including in regions where precipitation increases (Mankin et al., 2019). Regional hydrological modelling finds that green water flows historically dominate in the USA, that many lowlands are runoff-consuming sinks, and that hydrologic position within the river network strongly modulates water availability (Weiskel et al., 2014). Another regional analysis links intensified rainfall to shifts from soil storage(green water) to channelised flows (blue water), thus elevating erosion risk (Eekhout et al., 2018). Additional conceptual studies highlight that changes in catchment characteristics and processesmodulate runoff fractions beyond shifts in precipitation and evaporative demand (Yang et al., 2018).

However, past studies primarily emphasise changes in (Mankin et al., 2018, 2019). Other studies have analysed related forms of terrestrial water partitioning at regional to global scales and highlighted the roles of hydrologic setting, catchment characteristics, rainfall intensity, land-surface processes and land use in shaping how precipitation is divided between runoff, storage, and ecosystem water use

(Weiskel et al., 2014; Eekhout et al., 2018; Yang et al., 2018; Scheff et al., 2022; Althoff and Destouni, 2023). Together, these studies have improved understanding of individual water fluxes, specific processes, and regional partitioning behaviour. However, less is known about the projected global patterns of runoff–transpiration partitioning across vegetated land areas and the factors associated with the spatial patterns of these changes.

This study aims to assess where future changes favour blue or green water flows as separate responses to shifting hydroecological conditions, while paying little attention to precipitation partitioning and its underlying drivers at the global scale to support impact-relevant interpretation. To address this knowledge gap, we use the Blue-Green pathways and which climatic and hydroecological changes are associated with these shifts. To do so, we define the Blue–Green Water Share (BGWS), a metric that quantifies the relative proportion of precipitation partitioned into transpiration (green water flow) and runoff (blue water flow). Positive BGWS values indicate that a larger percentage of precipitation is partitioned towards runoff than towards transpiration, and vice versa for negative values (see Sect. 2.4). We focus on these flows as they represent key variables for understanding water availability – transpirationfor terrestrial ecosystems and rainfed agriculture, and runoff for aquatic ecosystems and human water withdrawals. BGWS thus provides a clear lens to assess patterns and future changes in green and blue water availability on global to continental scales, while enabling the analysis of associated controlling factors.

In this study, we partitioning of precipitation into runoff and transpiration. We analyse the historical distribution of BGWS (1985–2014) and its projected changes under the SSP3–7.0 scenario (2071–2100 minus 1985–2014) using an ensemble of ~~11~~ 12 ESMs participating in the Coupled Model Intercomparison Project Phase 6 (CMIP6; Eyring et al., 2016; Table S1). We

~~investigate the key controlling factors behind shifts in blue–green water partitioning by relating~~ then relate changes in BGWS to changes in mean and extreme precipitation, atmospheric water demand and cloud cover, soil moisture, and vegetation properties. Finally, we examine how BGWS changes co-occur with absolute changes in runoff and transpiration to provide a process-based interpretation of future changes in blue and green water availability and to discuss ~~the implications for water and land management~~ their implications in a warming, CO_2-enriched world.

2 ~~Methods~~Data and methods

2.1 ~~Climate~~ Earth system model data

We use output from ~~11~~ 12 CMIP6 ESMs ~~that provide the required variables~~ for both the historical experiment and the SSP3-7.0 scenario (Eyring et al., 2016) (Table S1). SSP3-7.0 represents a regional rivalry pathway (Shared Socioeconomic Pathway 3) with a radiative forcing of 7 Wm^{-2} by 2100 (Representative Concentration Pathway 7.0) (Fujimori et al., 2017; Riahi et al., 2017). We select SSP3-7.0 because ~~it offers the broadest availability of the variables required to compute the BGWS metric and to perform the subsequent analyses. This choice is further supported by recent evidence that the~~ the warmest scenario, SSP5-8.5, is unlikely to be realised under current and projected emission trajectories (Hausfather and Peters, 2020). SSP3-7.0, as the second-highest emission scenario, is therefore particularly relevant for current climate impact assessments. However, we acknowledge that hydroecological responses are scenario-dependent (Yang et al., 2018). Given the impact focus of our analysis, we prioritise a scenario whose coupled forcings ~~more directly inform hydroecological responses and~~ are more directly policy-relevant outcomes than idealised experiments.

The ESMs are selected to provide the variables required to compute the BGWS metric (Sect. 2.4) and the climatic and hydroecological variables used in the subsequent analyses (Sect. 2.5). Additionally, only models with time-varying leaf area index (LAI) were considered (Table S1). For each model, we select the ensemble member with the lowest available indices along the CMIP6 ensemble axes "ripf": realisation, initialisation, physics and forcing; member IDs in Table S1). This approach ensures that each model contributes equally to the analysis and avoids over-representing models with a larger number of ensemble members. ~~We analyse monthly mean output of the following variables: (1) total precipitation, *pr*; (2) near-surface air temperature, *tas*; (3) near-surface specific humidity, *huss*; (4) surface pressure, *ps*; (5) evapotranspiration, *evspsbl*; (6) transpiration, *tran*; (7) leaf area index, *lai*; (8) total-column soil moisture, *mrso*; (9) total runoff, *mrro*; and (10) gross primary productivity, *gpp*. In addition, we use daily total precipitation to calculate the extreme precipitation index RX5day (annual maximum consecutive five-day precipitation; Sect. 2.5).~~

~~We use total-column soil moisture to maximise the number of models included in the analysis. Because active soil hydrology depths differ among models, we evaluate percentage relative changes in total-column soil moisture rather than absolute values. For the historical analysis, we additionally utilise upper-soil moisture (0–10 cm), *mrsos*, for which the depth is uniform across models. However, because this shallow layer does not generally represent rooting depth, we retain total-column soil moisture for subsequent analyses.~~

~~Evaporation E is diagnosed as the non-transpirational component of evapotranspiration ET and transpiration E_t,~~

$E = \mathrm{ET} - E_t$.

~~This quantity represents the flux of water from liquid and solid phases to vapour from underlying surfaces, excluding transpiration. We do not use CMIP6 evaporation variables directly because key components (e.g. *evspsblsoi*) are unavailable for many models.~~

2.2 Observation-based and reanalysis datasets

To evaluate the performance of the selected CMIP6 models in representing the BGWS, we compare the ESM results against observation-based and reanalysis datasets. Specifically, we compute the BGWS from GPCC precipitation (Schneider et al., 2022), G-RUN runoff (Ghiggi et al., 2019), and GLEAM transpiration (Miralles et al., 2011), providing an observation-based reference for model evaluation. These datasets are derived using different methodologies: GPCC is a gauge-based precipitation dataset, G-RUN reconstructs global runoff using a machine-learning approach trained on streamflow observations, and GLEAM ~~estimates land surface evaporation~~ is a hybrid observation–model product that estimates land-surface evaporation and transpiration from satellite-based data~~, incorporating microwave soil moisture retrievals andthe Priestley-Taylor equation. Due~~ . Thus, these reference datasets are not equally direct observations and, due to their independent origins, ~~these datasets~~ are not fully consistent ~~, as they do not ensure a closed water balance at global scale~~with one another or with a closed global water balance (Huang et al., 2025). To account for this, we also use ERA5-Land, a physically consistent reanalysis dataset providing all required variables from a single modelling framework (Muñoz-Sabater et al., 2021). However, reanalysis data are not direct observations and inherit uncertainties from model physics, model parametrisations and input data quality. While ERA5-Land offers a spatially and temporally coherent dataset, its ability to accurately represent long-term hydrological changes remains uncertain (Dutta and Markonis, 2024). ~~To ensure comparability, we apply the same data processing and methodological steps to the observation-based and reanalysis datasets as to the CMIP6 model output over the~~ We therefore use these global-scale gridded datasets as a first-order consistency check of ESM simulated BGWS patterns, rather than as a full benchmarking of ESM skill. In addition to comparing climatological BGWS fields, we also assess whether the ensemble mean reproduces observed changes in BGWS over the recent historical period. For this purpose, we compare BGWS changes between 1985–1999 and 2000–2014 in the CMIP6 ensemble mean and the reference datasets.

2.3 Data preprocessing and multi-model ensemble

To enable spatial comparison across models and datasets, we regrid all fields to a common $1^\circ \times 1^\circ$ latitude–longitude grid using conservative interpolation. After regridding, we compute 30-year climatological means for a historical period (1985–2014) and a far-future period (2071–2100). Future-minus-historical changes are then calculated for all variables used in the subsequent analyses.

We apply a fixed historical mask derived from the ensemble mean over 1985–2014. The mask restricts the analysis to vegetated and hydrologically active land areas where the subsequent runoff–transpiration partitioning analysis is meaningful.

Grid cells are retained only where mean precipitation exceeds 0.05 $\mathrm{mm\,day^{-1}}$, mean runoff exceeds 0.005 $\mathrm{mm\,day^{-1}}$, mean transpiration exceeds 0.005 $\mathrm{mm\,day^{-1}}$, and mean LAI exceeds 0.3 $\mathrm{m^2\,m^{-2}}$. These thresholds are deliberately low screening thresholds rather than hydroclimatic regime definitions. They exclude grid cells with very small water inputs, negligible runoff or transpiration, or sparse vegetation. The same mask is applied consistently to all historical fields, future changes, and reference datasets.

We employ an unweighted multi-model ensemble (hereafter referred to as the ensemble mean) to mitigate uncertainties associated with individual model biases and initial-condition variability. For each model, climatological means and changes are first computed at the model level and then averaged across models to obtain the ensemble mean. This ordering ensures that ensemble statistics reflect individual model responses before averaging. We do not apply performance-based weighting, as our objective is to assess broad climate impacts rather than to optimise the ensemble for a specific variable. Spatial means are always calculated as area-weighted averages to account for the convergence of meridians with latitude. Each grid cell is weighted by the cosine of its latitude, $\cos(\varphi)$, where φ denotes latitude.

2.4 Blue–Green Water Share

~~We select runoff as the proxy for blue water flow and transpirationas a proxy for green water flow, recognising both flows as critical indicators of the volume of precipitation allocated to the distinct water resource components. Focusing on these water flows is further justified by their direct link to blue-green water partitioning, their capacity to capture key water cycle dynamics, and the valuable insights they provide even without detailed observations of storage dynamics (Wu et al., 2021).~~

In this study, we analyse blue–green water partitioning using precipitation (P; $\mathrm{mm\,day^{-1}}$) as the incoming water supply, runoff (R; $\mathrm{mm\,day^{-1}}$) as blue water flow and transpiration (E_t; $\mathrm{mm\,day^{-1}}$) as the vegetation-mediated green water flow in vegetated and hydrologically active land areas. We focus on transpiration because it represents the direct vegetation water-use response, whereas non-transpirational evaporation may respond differently to climate change than vegetation-mediated water use (Lawrence et al., 2007). This distinction matters because total ET can reflect offsetting changes in its components. For example, transpiration can decrease while soil evaporation increases, so the ET response emerges from opposing biological and physical processes (Berg and Sheffield, 2019). Using ET instead of transpiration would therefore address a different question, namely runoff versus total evaporative loss rather than runoff versus vegetation-mediated water use (Denissen et al., 2022).

We introduce BGWS as a flow-based partitioning metric for runoff and transpiration rather than as a complete representation of all blue and green water or water-balance components. BGWS thus does not represent total green water flow, but specifically the vegetation-mediated component of green water use captured by transpiration. The historical mask defined in Sect. 2.3 ensures that the metric is evaluated only in regions where this transpiration-based interpretation is meaningful.

We define the BGWS metric as:

$$\mathrm{BGWS} = \frac{R - E_t}{P} \times 100, \tag{1}$$

which is dimensionless and expressed in percent. Positive BGWS values indicate that a larger share of precipitation is partitioned towards runoff, whereas negative BGWS values indicate that a larger share is partitioned towards transpiration. BGWS

can thus be interpreted as the percentage imbalance of total precipitation between blue and green water flows. ~~A deviation of ±10 from equilibrium corresponds to a 10 % greater allocation of precipitation towards blue or green water, respectively.~~

BGWS is therefore complementary to existing partitioning metrics. Relative to the blue water trade-off (BWT) metric used by Mankin et al. (2018, 2019), BGWS contrasts runoff directly with transpiration, does not include interception or storage terms, and reports the result as a normalised share of precipitation. Thus, interception-driven canopy effects are not represented explicitly by BGWS. For assessing vegetation-mediated green water use, however, transpiration as a direct ESM output is useful because it provides an immediate indicator of plant water use.

We focus on water fluxes rather than water stores because hydrological fluxes are more consistently available and more directly comparable across the selected CMIP6 ESMs. Moreover, on multi-decadal timescales (here, 30-year means), storage changes tend to be small relative to fluxes, as ~~most catchments approach approximate steady~~ many catchments approach a near-steady state within this period (Han et al., 2020). Neglecting storage terms therefore provides a pragmatic and interpretable framework for large-scale analysis, although this simplification remains a limitation and an avenue for future research.

Changes in BGWS, denoted as ΔBGWS, indicate shifts in blue–green water partitioning and are calculated as

$$\Delta\mathrm{BGWS} = \mathrm{BGWS}_{\mathrm{Future}} - \mathrm{BGWS}_{\mathrm{Historical}}. \tag{2}$$

A positive ΔBGWS reflects an increasing partitioning towards blue water flow, whereas a negative ΔBGWS indicates an increasing partitioning towards green water flow. Although ΔBGWS does not directly measure ~~variations in green and blue water flows, they provide a clear depiction of the~~ absolute changes in all blue and green water components, it provides a clear measure of the changing trade-off between ~~these components~~runoff and transpiration.

2.5 ~~Climate indices and derived variables~~Climatic and hydroecological variables

We analyse both the historical 30-year climatological means and the future-minus-historical changes in selected climatic and hydroecological variables associated with the distribution and shifts in blue–green water partitioning. The selected variables are mean precipitation (P; $\mathrm{mm\,day^{-1}}$), precipitation seasonality (P_{seas}; $\mathrm{mm\,day^{-1}}$), annual maximum consecutive five-day precipitation (RX5day; mm), surface soil moisture ($\mathrm{SM_{surf}}$; mm), leaf area index (LAI; $\mathrm{m^2\,m^{-2}}$), transpiration-based water-use efficiency (WUE; $\mathrm{gC\,m^{-2}\,mm^{-1}}$), mean vapour pressure deficit (VPD; hPa), VPD seasonality ($\mathrm{VPD_{seas}}$; hPa), and total cloud cover (CLT; %). Except for RX5day, which is derived from daily precipitation, all variables are based on monthly mean output. The variable selection is based on the predictor screening described in Sect. 2.6. Seasonality, RX5day, VPD, and WUE are computed as follows.

Precipitation and VPD seasonality are defined as the standard deviation of the 12 monthly climatological means within each 30-year period. For a given variable X and monthly climatology $\overline{X}_m$, seasonality is computed as

$$X_{\mathrm{seas}} = \sqrt{\frac{1}{12}\sum_{m=1}^{12}\left(\overline{X}_m - \overline{X}\right)^2}, \tag{3}$$

where $\overline{X}_m$ is the climatological mean for month m and $\overline{X}$ is the mean of the 12 monthly climatological values.

RX5day is derived from daily precipitation as the annual maximum consecutive five-day precipitation. For a given year j,

$$\text{RX5day}_j = \max(RR_{kj}), \tag{4}$$

where RR_{kj} denotes total precipitation accumulated over any five-day interval ending on day k within year j. For each 30-year period, RX5day is averaged over the annual maxima.

VPD is calculated using the Buck equation (Buck, 1981) to estimate saturation vapour pressure (e_s),

$$e_\mathrm{s} = 611.21 \times \exp\left[\left(18.678 - \frac{T}{234.5}\right)\left(\frac{T}{257.14+T}\right)\right], \tag{5}$$

where T is near-surface air temperature in °C, and 611.21 Pa is the saturation vapour pressure at 0 °C. Actual vapour pressure (e_a) is obtained from specific humidity (q) and surface pressure (p_s, in Pa) as

$$e_\mathrm{a} = \frac{q\,p_\mathrm{s}}{0.622 + 0.378\,q}, \tag{6}$$

and VPD is then given by

$$\text{VPD} = e_\mathrm{s} - e_\mathrm{a}. \tag{7}$$

VPD is converted from Pa to hPa for the analysis.

We use the ratio of gross primary productivity (GPP) to transpiration to compute WUE, a widely used proxy for the CO_2 effect on stomatal resistance (Keenan et al., 2013; Lian et al., 2021; Ruehr et al., 2023):

$$\text{WUE} = \frac{\text{GPP}}{E_\mathrm{t}}, \tag{8}$$

which quantifies the efficiency of carbon assimilation per unit of water consumed by vegetation through transpiration.

2.6 Multiple regression analysis

~~Predictor variables are chosen to represent hydroecological processes relevant to climate-change impacts and to allow physical interpretation of their influence on ΔBGWS. We use changes in mean precipitation (ΔPR)and extreme precipitation (ΔRX5day) to capture long-term moisture availability and short-term hydrological extremes. Changes in vapour pressure deficit (ΔVPD) represent atmospheric dryness and plant physiological stress, while changes in soil moisture (ΔSM) reflect land-surface water availability. Vegetation dynamics, including biophysical changes and CO_2 fertilisation effects, are represented by changes in leaf area index (ΔLAI)~~

We construct multiple linear regression (MLR) models ~~separately for each historical BGWS regime to assess how these hydroecological drivers affect ΔBGWS, using MME mean changes in the predictors. Prior to fitting, each predictor is scaled by its maximum absolute value (maximum scaling), such that each feature is bounded by $[-1, 1]$. The response variable ΔBGWS is left on its original scale. The dataset is split into 70 % trainingand 30 % testing subsets.~~ with Elastic Net regularisation separately for the two historical BGWS regimes to explain the spatial pattern of projected ΔBGWS across grid cells. Each grid

cell is treated as one sample, and both the predictors and the response variable are based on ensemble mean changes between the future and historical periods. The analysis therefore explains spatial differences in projected ΔBGWS within each regime. It does not attribute the temporal evolution of BGWS at individual grid cells or regions.

Because neighbouring grid cells are not independent, we apply spatially blocked cross-validation. Grid cells are grouped into $10^\circ \times 20^\circ$ latitude–longitude blocks, and all model training, tuning, and testing are performed using these spatial blocks as groups. For each regime, we apply repeated grouped train–test splits with 20% of the spatial blocks held out per repeat, combined with nested grouped cross-validation for Elastic Net hyperparameter tuning. To favour simpler models and reduce overfitting, the final hyperparameters are selected using a one-standard-error rule. Model performance is evaluated using out-of-sample R^2 on held-out spatial blocks.

To address multicollinearity among predictors and to regularise the regression, we apply Elastic Net regularisation (Friedman et al., 2010). The Elastic Net objective function is

$$\min_{\boldsymbol{\beta}} \left[\frac{1}{2n} \sum_{i=1}^{n} (y_i - \hat{y}_i)^2 + \alpha\rho \sum_{j=1}^{p} |\beta_j| + \frac{\alpha(1-\rho)}{2} \sum_{j=1}^{p} \beta_j^2 \right], \tag{9}$$

where y_i and $\hat{y}_i$ are the observed and predicted values, n is the number of ~~observations~~samples, β_j are the regression coefficients, α controls the overall regularisation strength, and ρ determines the balance between L1 (Lasso) and L2 (Ridge) penalties~~, ranging from 0 (pure Ridge) to 1 (pure Lasso). The first term measures model fit via the residual sum of squares. The~~ . The L1 penalty promotes sparsity by shrinking some coefficients to exactly zero, ~~thereby facilitating feature selection,~~ whereas the L2 penalty shrinks coefficients towards zero without eliminating them, helping to stabilise estimates under multicollinearity. Prior to model fitting, all predictors are standardised to zero mean and unit variance within each training split, while ΔBGWS is left on its original scale.

~~We select α and ρ using 5-fold cross-validation on the training data, evaluating a predefined grid of hyperparameter combinations and choosing the configuration that maximises the coefficient of determination (R^2). After selecting the optimal hyperparameters, the model is retrained on the full training dataset. Predictive performance and generalisability are then assessed on the testing subset using R^2.~~ The final predictor set was selected from a larger initial set of candidate predictors according to their contribution to predictive performance, their physical interpretability, and data availability across the full 12-model ensemble (Sect. S2). The final set includes changes in mean precipitation, precipitation seasonality, RX5day, mean VPD, VPD seasonality, total cloud cover, near-surface soil moisture, LAI, and WUE. Together, these variables represent climatic and hydroecological processes relevant to climate change impacts and allow physical interpretation of their influence on ΔBGWS. Changes in mean precipitation, precipitation seasonality, and extreme precipitation represent water supply and hydrological extremes. RX5day is used as the main extreme precipitation metric because multi-day precipitation accumulation shows slightly better spatial agreement than single-day extremes in CMIP6 and observational evaluations, making it a more robust indicator of extreme precipitation in large-scale datasets (Li et al., 2021a; Dunn et al., 2022). Changes in mean vapour pressure deficit and VPD seasonality represent atmospheric dryness and plant water stress. Changes in near-surface soil moisture represent surface water availability, while changes in LAI and WUE represent vegetation state and plant physiological

responses to elevated CO_2. Changes in LAI reflect both climatic and human influences, including land-use and land-cover change, although these contributions are not isolated explicitly here. Changes in total cloud cover represent an additional atmospheric control related to energy and moisture conditions.

To quantify the contribution of each predictor to model performance, we compute permutation importance scores (Breiman, 2001). This model-agnostic metric is obtained by randomly permuting the values of a given predictor and quantifying the resulting change in R^2. For each ~~predictor, we perform~~ repeat and each predictor, predictor values are permuted 20 ~~permutations in both the training and testing datasets and aggregate the corresponding importance scores. Applying the method to both training and testing data allows us to compare model behaviour on seen and unseen data. However, we primarily interpret importance scores derived from the testing data~~ times and the resulting decrease in R^2 is recorded. We interpret these test-set importance scores as measures of ~~out-of-sample predictor relevance for ΔBGWS. In some cases, the decrease in R^2 associated with permuting a predictor can exceed the model's baseline R^2, indicating that the model's performance drops below that of a mean-only benchmark when the information in that predictor is destroyed. This does not imply that the model relies exclusively on a single predictor, but rather highlights its strong contribution to predictive skill.~~ the contribution of each predictor to the spatial pattern of projected ΔBGWS within each regime. For comparison with the ensemble-mean attribution, we repeat the same blocked regression workflow for each individual ESM and report individual-model permutation importances only where mean held-out $R^2 > 0.3$.

3 Results and discussion

3.1 Historical distribution of BGWS

~~Figure 1a shows the global distribution of the BGWS for the historical period (1985-2014), based on the multi-model ensemble mean . Land fractions with greater shares of blue water (blue water regime)~~ The historical BGWS pattern in the CMIP6 ensemble mean (1985–2014; Fig. 1a) reveals three overarching features: energy-limited, water-limited, and precipitation-seasonality regulated blue–green water partitioning. The first two features are consistent with the broader literature distinguishing energy- and ~~green water (green water regime) are equally distributed~~water-limited land-surface or ecosystem regimes, while the third extends this logic to precipitation-seasonality effects that are particularly relevant for blue–green water partitioning (Seneviratne et al., 2010; Denissen et al., 2022). On average, ~~$\sim$ 3 % more of the global land~~ the area-weighted BGWS is slightly positive, indicating that ~ 2 % more precipitation is partitioned towards blue water flow, with notable ensemble variability from ~~-6% to +14%~~ -16 % to $+15$ % (Table S4). These contrasts stem from differences in the model representation of precipitation characteristics, land-surface hydrology, and vegetation dynamics, which contribute to well-documented CMIP6 biases in simulated land-surface water fluxes relative to reference products (Clark et al., 2015; Gentine et al., 2019; Zheng et al., 2019; Li et al., 2021b; Padrón et al., 2022; Yang et al., 2023).

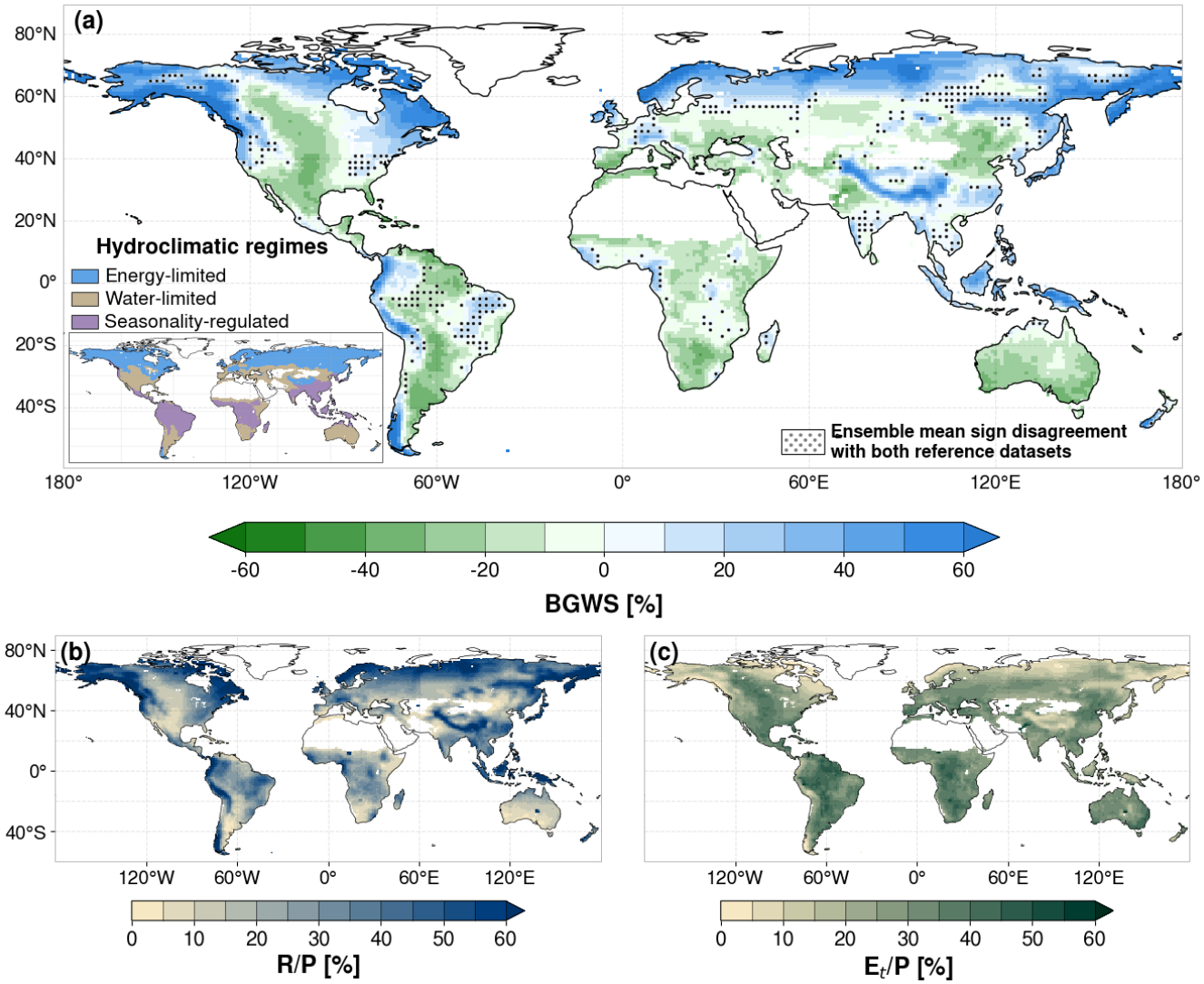

Figure 1. Ensemble mean for the historical period (1985–2014) based on 12 CMIP6 Earth system models. (a) BGWS [%] with inset showing a simple hydroclimatic regime classification in which each grid cell is assigned to the regime with the strongest standardized signal of low near-surface soil moisture, low air temperature, or high precipitation seasonality. (b) runoff share, R/P [%], and (c) transpiration share, E_t/P [%]. Blue colours in the BGWS colour map indicate a greater partitioning of precipitation towards runoff (blue water flow), whereas green colours indicate a greater partitioning towards transpiration (green water flow). Dots in panel (a) indicate regions where the sign of the ensemble mean BGWS disagrees with both reference datasets.

Comparing the spatial pattern of the ensemble mean BGWS with observation-based and reanalysis products indicates a reasonable large-scale representation for the historical climatology(Fig. S1). Agreement is weaker, but still qualitatively similar, for recent historical changes over the shorter evaluation period (Fig. S2). ~~Yet, the absolute~~ Compared with both reference

datasets, the ensemble mean BGWS values are biased towards too much blue water. Decomposing BGWS into runoff (R/P) and transpiration (E_t/P) ratios shows that ~~both components contribute to this bias . The ensemble mean largely underestimates T/P~~ the bias is driven primarily by underestimated E_t/P (negative mean offset)~~and modestly overestimates Q/P (positive mean offset) (Figs.S3 and S4).~~ , while regional differences in R/P also contribute (Figs. S3 and S4). One possible structural contribution to the underestimated E_t/P bias is the limited representation of lateral groundwater redistribution in many large-scale land models used in ESMs, where this process is often overlooked or strongly simplified. By underrepresenting shallow groundwater support to ET in drylands or during dry periods, this may partly favour a more blue-biased BGWS (Maxwell and Condon, 2016; Liao et al., 2025). Accordingly, we treat BGWS as a process indicator and base interpretation primarily on directional patterns, sign-robust spatial structures, and covariation with relevant predictors, while avoiding detailed interpretation in regions with disagreement against both reference datasets (dots in Fig. 1a).

Energy-limited blue–green water partitioning, the first BGWS feature, is dominant across higher latitudes ($> 60°$N) and high-altitude regions, which consistently show greater partitioning towards blue water flow (Fig. 1a). This pattern aligns with the Budyko framework, which links energy-limited conditions to increased runoff (Budyko, 1974). In the higher latitudes, ~~94~~95% of the land area exhibits a larger blue water share, with an area-weighted mean BGWS of ~~+40%~~+36 %. Here, low net radiation (light-limited) and low air temperatures (kinetic/phenology-limited) ~~result in below-average gross primary productivity (GPP) and transpiration (Figs.1d~~ coincide with below-global-average E_t/P, while near-surface soil moisture remains comparatively high (Figs. 1c and S5)~~, while near-saturated soil moisture likely persists~~. Consequently, precipitation predominantly contributes to runoff (Fig. 1b~~,c). Furthermore, mountain ranges exhibit distinct precipitation and runoff patterns. Here,~~). Mountain ranges exhibit similar behaviour, where orographically enhanced precipitation and topography-controlled runoff parametrisations in ESMs (e.g., SIMTOP) ~~cause~~ can contribute to larger blue water shares (Niu et al., 2005; Gnann et al., 2025). ~~Additionally, in both higher latitudes and high-altitude regions, snowmelt-driven~~ Snowmelt-driven runoff likely further enhances blue water shares in cold regions (Barnett et al., 2005), although ~~ongoing~~ simplified representation of snow sublimation in ESMs may also contribute to runoff overestimation in some high-altitude regions and thus reinforce locally blue-biased partitioning (Stigter et al., 2018). Ongoing warming-related snow cover loss, by contrast, increases net radiation and ET and can reduce runoff (Milly and Dunne, 2020). Energy-limited partitioning is also evident across parts of the mid-latitudes (40–60° N/S)~~. Contrary to~~ , but with much smaller positive BGWS values than in the higher latitudes, ~~these regions show a smaller blue water share with a zonal~~ with an area-weighted mean BGWS of ~~$\sim +6$ %, likely due to seasonal contrasts~~ about $+4$ %. This is consistent with seasonal transitions between winter energy limitation and summer water limitation ~~(Knoben et al., 2018). Note that, compared~~ (Seneviratne et al., 2010; Knoben et al., 2018). Compared with observation- and reanalysis-based products, however, the ensemble mean tends to overstate both the magnitude and the spatial extent of blue water shares in energy-limited high- and mid-latitudes (Fig. S1).

~~Water-limitation regulated~~ Water-limited blue–green water partitioning, the second BGWS feature, dominates in ~~global drylands~~ semi-arid and dry sub-humid regions such as the Eurasian Steppe or Australia's Outback (Fig. 1a). These water-limited environments are marked by annual precipitation below the global mean and relatively low near-surface soil moisture (Fig. S5). Despite these hydrological constraints, these ecosystems partition a larger fraction of available water towards

transpiration, increasing the green water share in line with observation-based data (Figs. 1 and S1). ~~While consistently low precipitation typically favours green water dominance, infrequent but intense rainfall in dryland regions can periodically trigger high surface runoff~~ The RX5day-to-annual-precipitation ratio is elevated across many of these dryland regions (Fig. S6)~~. This mechanism is most evident over the Sahara, where the high ratio of RX5day to annual precipitation is associated with larger blue water shares (Figs. 1a and S6). Yet, runoff parameterisation in CMIP6 land-surface schemes emphasise saturation-excess and under-represent infiltration-excess runoff, which may explain why Saharan blue water dominance is more pronounced in observation-based products (Hou et al., 2023) (Fig. S1).~~ , indicating that rainfall is often temporally concentrated even where mean precipitation is low. Nevertheless, within the retained vegetated drylands, the annual partitioning still tends to favour transpiration over runoff. This is consistent with water-limited ecosystems maintaining relatively low runoff fractions while using a large share of the limited incoming precipitation for vegetation water use (Althoff and Destouni, 2023).

~~Precipitation-intensity regulated~~ Precipitation-seasonality regulated blue–green water partitioning, the third BGWS feature, emerges ~~in the humid subtropical and tropical regions. Larger blue water shares occur where high mean and intense precipitation (RX5day) keep the upper soil near saturation more often. This yields higher saturation-excess runoff for a given transpiration demand. In contrast, in humid regions where mean and intense precipitation are insufficient to maintain wet upper soils, saturation events are rarer and partitioning shifts toward green water. This asymmetric feature can be observed when comparing the major rainforests (~~most clearly in monsoonal and other strongly seasonal climates highlighted by the inset in Fig. 1a~~). While the rainforests of northern South America and central Africa primarily favour green water dominance, the Southeast Asian rainforest demonstrates a contrasting pattern. Transpiration is of similar magnitude across the major rainforests (Fig. 1d). Hence, this BGWS asymmetry is likely due to Southeast Asia receiving more mean and intense precipitation associated with stronger Monsoon rains,~~ . In these regions, BGWS depends not only on how much precipitation falls annually, but also on how strongly rainfall is concentrated within the year. Regions with high precipitation seasonality, such as southern and eastern Asia and ~~corresponding higher upper soil moisture~~ parts of the Maritime Continent, tend to show larger blue water shares where wet-season rainfall is strongly concentrated, RX5day is high, and near-surface soil moisture is comparatively high (Figs. 1 and S5). ~~Assuming broadly similar soil properties across rainforests, more frequent near-saturation in Southeast Asia generates more saturation-excess runoff and larger blue water shares (Fig. 1a, c). Compared with observation-based products, this rainforest asymmetry differs, with the Amazon showing slightly larger blue water shares (Fig. S1).~~

~~Similarly, subtropical regions~~By contrast, humid regions with more weakly seasonal rainfall, such as much of the Amazon and central Africa, tend to show larger green water shares and higher E_t/P. Thus, the contrast is not simply between wet and dry regions, but between climates with strongly concentrated wet seasons and those with more even rainfall distribution. This mechanism is also consistent with the contrast between East Asian monsoon regions, which show larger blue water shares, and subtropical regions such as the Florida Peninsula, where more evenly distributed rainfall coincides with ~~relatively high mean precipitation and RX5day, such as southern China and southern Japan – both influenced by the East Asian Summer Monsoon – experience higher upper soil moisture and corresponding elevated runoff (Figs. 1b,c and S5). Consequently, these regionsexhibit greater partitioning towards blue water flows (Fig. 1a). In contrast, subtropical regions with~~ larger green water shares~~, such as the Florida Peninsula, mostly exhibit lower mean and intense precipitation with correspondingly drier upper~~

soils and reduced runoff, while transpiration remains at levels comparable to , e.g., southern China (Fig. 1 and S5). This green water dominance may also be influenced by rainfall distribution, as more evenly spread precipitation can sustain higher transpiration throughout the year. Notably, significant ensemble disagreement exists .

Overall, the historical BGWS distribution is therefore consistent with a transition from energy-limited blue-water dominance in cold and high-altitude regions, to water-limited green-water dominance in semi-arid regions, and to seasonality-regulated partitioning in monsoonal and humid subtropical climates. Several regions, especially within this third feature, also show disagreement with both reference datasets or elevated ensemble spread, underscoring the challenges ESMs still face in representing humid subtropical and tropical hydroecological dynamics (Fiedler et al., 2020; Padrón et al., 2022; Figs. 1a and S7).

3.2 Projected changes in BGWS

Figure 2a maps the projected BGWS changes (2071-2100 minus 1985-2014) under the regional rivalry scenario (SSP3-7.0), categorising grid cells based on whether they have a positive or negative historical BGWS. The figure highlights either a strengthening or weakening of the existing separated by whether grid cells historically belong to the blue or green water regime, with each of these four trends covering similar proportions of the global land area(Table S3). Notably, a regime shift from blue towards green water is projected in 4% of global land area, while the reverse is simulated in 6.3% (Fig. S8 and Table S4). The balanced distribution of global BGWS trends cancel out opposing changes, yielding no discernible mean trend. However, individual model projections vary considerably, with . The four change classes occupy broadly comparable fractions of the analysed land area. In the historical green water regime, 23% becomes greener and 33% less green; in the historical blue water regime, 20% becomes bluer and 24% less blue. Despite this broad balance in areal coverage, the ensemble-mean global BGWS increases slightly by $+1.23$ ppts (Table S4), with individual-model global mean changes ranging from -2% to +5% (Table S4).

In the higher latitudes ($> 60°$N), equal land areas (~ 50 %) experience amplification -1.89 to $+4.99$ ppts. Regime shifts are less extensive than the strengthening or weakening of the historical blue water regime existing regimes, and occur more often from green to blue than from blue to green (Fig. 2a). Despite ensemble variability, robust S8). Because BGWS reflects the difference between runoff and transpiration relative to precipitation, a larger blue water share increases are present in, e.g., Alaska, strongly associated with enhanced precipitation arises wherever runoff changes more positively than transpiration, whereas a larger green water share arises wherever transpiration changes more positively than runoff. The spatial expression of these mechanisms varies strongly across latitude bands and climate regimes (Fig. 2a,b). In contrast, areas with a robust increase in the green water share, e.g., northwestern Eurasia , are strongly linked to expanding leaf area (Fig. S9). Here, rising transpiration demand exceeds additional precipitation supply, resulting in increasing green water shares).

Larger blue water shares most directly occur where runoff increases more than transpiration increases. This pattern is evident in wetter parts of the historical blue water regime, for example, in northeastern Eurasia and along the East Asian monsoon belt, where enhanced precipitation coincides with increasing runoff and a strengthening of blue-water dominance (Fig. 2). Although a larger share of precipitation is partitioned towards green water flow, these regionsconcurrently experience an increase in blue

water flow (Fig. 2c; see also In these regions, both blue and green water flows increase in absolute terms, but runoff gains are larger, so partitioning shifts further towards blue water. Similar positive BGWS changes are also visible in historically blue-water dominated tropical regions such as large parts of India, where future trends are generally positive and coincide with increased wetting (Fig. S9 for relative changes). This highlights the function of the BGWS metric, which emphasizes changes in water partitioning rather than absolute shifts in water availability (see Sect. 3.4). 2).

Unlike the balanced BGWS response in higher latitudes, 73% of mid-latitudes experience

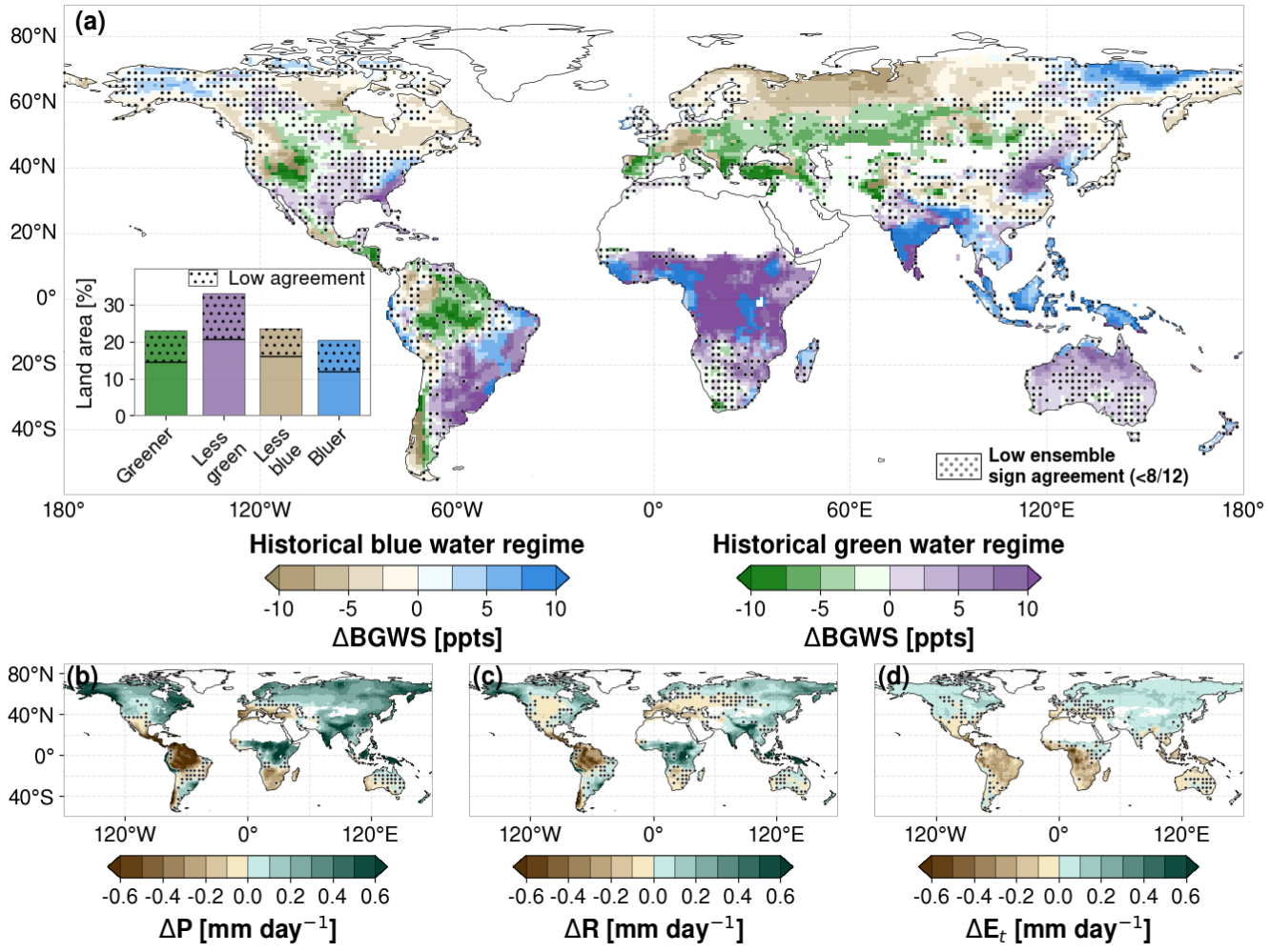

Figure 2. Ensemble mean change (2071–2100 minus 1985–2014) under the SSP3-7.0 scenario based on 12 CMIP6 Earth system models. (a) ΔBGWS [ppts], shown separately for grid cells with historically positive BGWS values (blue water regime; beige to blue colours) and historically negative BGWS values (green water regime; green to purple colours). Blue and purple colours indicate shifts towards larger blue water shares, whereas green and beige colours indicate shifts towards larger green water shares. The inset summarises the analysed land-area fractions of the four BGWS-change classes; bar heights show the total area of each class, the horizontal line marks the fraction with robust sign agreement, and the stippled upper part indicates the fraction with low model agreement. (b) Δ precipitation [$\mathrm{mm\,day^{-1}}$], (c) Δ runoff [$\mathrm{mm\,day^{-1}}$], and (d) Δ transpiration [$\mathrm{mm\,day^{-1}}$]. Stippling marks regions of low inter-model agreement, where fewer than 8 of the 12 models agree on the sign of change.

Larger blue water shares can also occur where runoff increases while transpiration decreases. This pattern is especially relevant in parts of the subtropics and tropics, where wetter conditions and increasing runoff coincide with declining transpiration. The major rainforests exhibit an asymmetric response in this respect: only the Amazon rainforest tends towards a greater green

water share~~increases, associated with substantial vegetation growth (Fig. S9). In some regions, e.g., central Europe, this green water gain coincides with runoff loss~~ , whereas parts of central Africa and Maritime Southeast Asia shift towards greater blue water shares. This divergence coincides with precipitation and runoff increases in the latter two regions, while transpiration declines across all three rainforest regions (Fig. 2~~c). Most mid-latitude regions with increasing~~). Consistent with these regional examples, 68% of the analysed subtropical land and 77% of the analysed tropical land are projected to experience larger blue water shares~~also show rising runoff (e.g., the mid-latitude East Asian monsoon belt; Fig. 2a). However,~~ .

A third pathway to larger blue water shares occurs where both runoff and transpiration decrease, but transpiration declines more strongly than runoff. This mechanism is visible in scattered historically water-limited patches of the subtropics and mid-latitudes, for example in parts of ~~the historically water-limited West North Central U.S. and the Canadian Prairies~~ eastern Australia and northwestern Mexico (purple in Fig. 2a)~~, blue water shares increase because transpiration decreases more than runoff (Fig. 2c, d). A similar pattern of blue water share increases occurs in subtropical patches in e.g. Mexico and Australia, where~~ . In these regions, the relative decline in transpiration exceeds ~~runoff loss (Fig. 2c, d)~~the runoff loss, shifting partitioning towards blue water even though absolute blue water flow may also decline. This contrasts with observed CO_2-driven blue water losses where greening increased ET and reduced streamflow in Australia's sub-humid/semi-arid basins (Ukkola et al., 2016)~~)~~ , and with vegetation-driven runoff declines in the American West (Mankin et al., 2017, 2019). ~~Over Australia, however, our result is consistent with ESM projections of increased runoff partitioning under CO_2 forcing (Mankin et al., 2019). While the LAI primarily increases in response to CO_2 fertilisation, transpiration decreases as higher WUE offsets~~ While LAI increases across many of these regions, transpiration does not always rise in parallel because higher WUE can offset rising water demands (Figs. 2d and S9). ~~Nonetheless, large areas are projected to experience blue water loss, as receiving a larger share of precipitation does not offset the overall decline in blue water (Fig. 2c). The responses to elevated CO_2 effects on hydrological processes should, however, be interpreted with caution given the considerable variability in CMIP6 models (Wei et al., 2024). Moreover, plants' water savings due to increased WUE do not always prevail. Southern Europe, for instance, is characterised by a greater reduction in runoff compared to transpiration, hence, experiencing a green water share increase (Fig. 2).~~More generally, whether dry regions will experience a blue or green water share increase depends largely on the interplay between rising vegetation water demand and WUE-related transpiration limitations~~. In the subtropics, 60% of the land area is projected to experience a greater blue water share, dominated by already wet regions, e.g., in Eastern Asia. Additionally, vegetation responses influence subtropical BGWS trends, though~~ , although structural uncertainties remain in how models represent vegetation responses to rising CO_2 and the resulting water-cycle impacts (Wei et al., 2024; Yang et al., 2021; Forzieri et al., 2020; Yang et al., 2023).

~~The BGWS response in humid subtropical and tropical regions remains highly sensitive to precipitation patterns and extremes. The major rainforests exhibit an asymmetric response, with only the Amazon rainforest showing an increasing green water share. In contrast, the Central African and Southeast Asian rainforests are projected to shift towards a greater blue water share . This divergence aligns with precipitation and runoff trends – both decreasing over the Amazon but increasing in the other two regions, while transpiration declines across all three~~ Larger green water shares occur where transpiration increases more than runoff increases. This mechanism is apparent in parts of the higher latitudes and mid-latitudes where leaf

area expands and transpiration gains exceed the concurrent runoff increase, for example in northwestern Eurasia (Fig. S9). Consistent with this pattern, 62% of the analysed land area north of 60°N experiences a weakening of the historical blue water regime. Although a larger share of precipitation is partitioned towards green water flow, these regions concurrently experience an increase in blue water flow (Fig. 2c). In such cases, the shift towards green water does not necessarily imply a drying climate, but rather that transpiration becomes relatively more important than runoff.

A larger green water share can also arise where transpiration increases while runoff decreases. This pattern is particularly evident in parts of eastern Europe, where greener partitioning coincides with runoff loss (Fig. 2). In ~~other tropical regions with a positive historical BGWS, e.g., large parts of India, future trends are generally positive, driven by increased wetting and scattered decreases in transpiration~~ such cases, vegetation gains and enhanced transpiration shift the balance towards green water while blue water availability declines in absolute terms. The same logic applies to other mid-latitude regions where warming- and CO_2-driven vegetation responses amplify transpiration despite weak or negative runoff trends.

Finally, larger green water shares occur where both runoff and transpiration decrease, but runoff declines more strongly than transpiration. This mechanism is evident in parts of southern Europe, where a greater reduction in runoff compared to transpiration results in a green water share increase (Fig. 2). ~~Overall, a majority (73%) of tropical land is projected to experience greater blue water shares, highlighting vegetation's response to rising CO_2 as a key factor amid contrasting trends in transpiration~~This mechanism is also relevant in other regions with blue water losses, as receiving a smaller or only slightly larger share of precipitation does not offset the overall decline in runoff.

3.3 ~~Extreme precipitation strongly impacts global~~ Climatic and hydroecological predictors of projected BGWS change

~~Precipitation partitioning changes between blue and green water flows are driven by various climatic and non-climatic factors. Our analysis of historical characteristics and projected changes in BGWS presents a unique opportunity to uncover key controlling factors behind shifts in blue-green water partitioning. We hypothesize that these shifts originate from alterations in~~ The regional BGWS changes described above suggest that future blue–green water partitioning reflects competing effects of changes in mean and extreme precipitation, changes in atmospheric and soil-moisture conditions, and vegetation responses. To quantify ~~their impacts, we performed~~ which selected predictors best explain the spatial pattern of ΔBGWS within each historical regime, we fitted separate blocked multiple linear regression (MLR) ~~analyses for each BGWS regime (Methods).~~ models for the historical blue and green water regimes (Sect. 2.6). Figure 3 summarises the resulting permutation importance scores for the ensemble mean together with the corresponding importance ranks from individual ESMs. Both MLR models ~~exhibit moderate predictive power (Fig. 3a,b). However, consistent variable importance rankings across training and testing datasets suggest robust and interpretable results (Breiman, 2001) (Fig. S10). We validate our approach by comparing MLR importance rankings with those from random forest models. The similarity in results between these two independent methods supports the robustness of our findings~~ show moderate to strong predictive skill ($R^2 = 0.49$ for the historical blue water regime and $R^2 = 0.72$ for the historical green water regime). This interpretation and the importance rankings are further supported by the nonlinear Random Forest sensitivity analysis (Fig. S10).

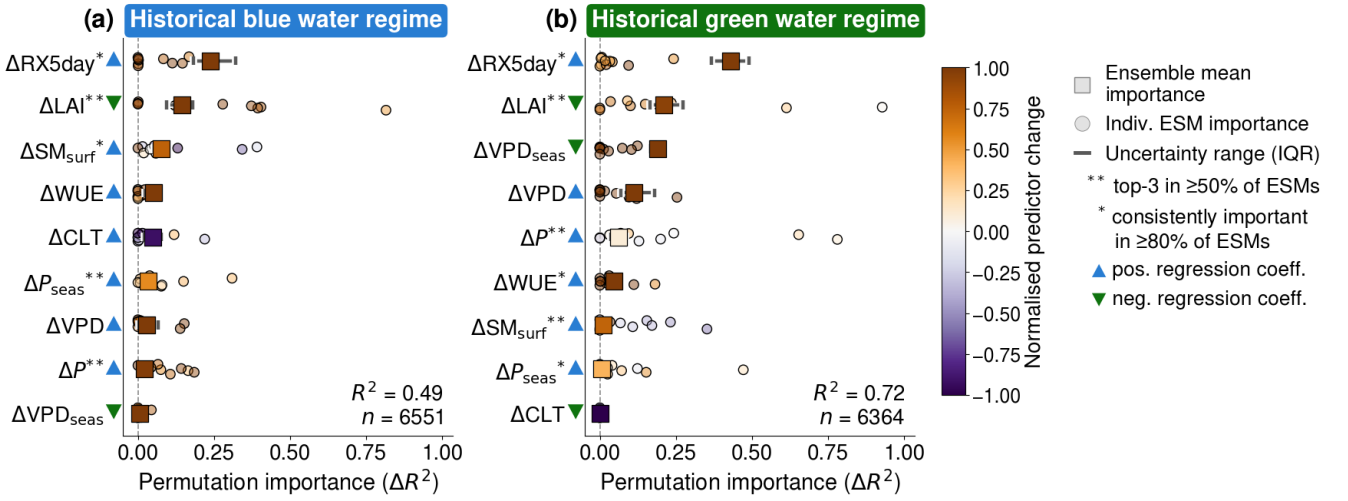

Figure 3. Variable importance for the spatial attribution of projected changes (2071–2100 minus 1985–2014) in ΔBGWS under the SSP3-7.0 scenario in the two historical BGWS regimes shown in Fig. 2: (a) historical blue water regime and (b) historical green water regime. Squares show the median permutation importance (ΔR^2) of the 12-model CMIP6 ensemble mean for the predictor set, and horizontal lines show the interquartile range across repeated blocked cross-validation splits. Circles show the median permutation importance from individual ESMs with mean model performance $R^2 > 0.3$. Colours indicate the normalised mean change of each predictor within the respective regime. Upward blue triangles indicate positive regression coefficients and downward green triangles indicate negative regression coefficients in the ensemble mean. Reported R^2 values give the mean model performance, and n is the number of grid cells in each regime.

Our results demonstrate that BGWS alterations in both regimes are most sensitive to extreme five-day precipitation changes (Fig. 3). RX5day is projected to increase across most of the global land area (Fig. S9), consistent with theoretical expectations that warming-driven increases in atmospheric moisture intensify precipitation extremes (Trenberth, 2011; Donat et al., 2016; Tabari, 2020). Its positive regression coefficient indicates that increases in RX5day ~~contributes to~~ are associated with larger blue water shares. This ~~relationship arises as high precipitation amounts over short periods~~ statistical relationship is physically plausible, because more intense multi-day rainfall can quickly saturate soils, triggering saturation-excess runoff in CMIP6 land-surface schemes. The RX5day effect would likely be even larger in models that also represent infiltration-excess runoff, which only a few schemes currently include (Hou et al., 2023). Additionally, ~~stormier conditions typically increase cloud cover, which reduces incoming shortwave radiation and thereby transpiration. This energy constraint may further reinforce the positive association between higher RX5day and larger blue water shares (Wang et al., 2023)~~current coarse-resolution ESMs tend to underestimate precipitation extremes and often exhibit drizzle bias, suggesting that the hydrological influence of RX5day may be underestimated in our analysis (Brunner et al., 2025). The individual ESMs show that ΔRX5day is an important predictor across most of the ensemble, but not consistently one of the top three predictors. This indicates that its dominance is strongest for the ensemble-mean BGWS field, whereas individual-model importance rankings are more variable. Such smoothing of model-specific noise and internal variability is a known consequence of multi-model averaging and helps isolate the common large-scale forced response, although it can also mask structural differences among models (Knutti et al., 2010).

Our findings emphasize two key points. First, ~~while mean precipitation might regionallydecrease, the intensification of intense rainfall (~~even where mean precipitation decreases regionally, stronger increases in RX5day ~~) induces the mean blue water share to rise~~can still shift BGWS towards larger blue water shares. This suggests ~~an intensification of runoff events even when the~~ higher runoff sensitivity to intense rainfall even where average runoff is decreasing. ~~Although more precipitation is thus periodically partitioned towards blue water, questions remain about its accessibility under climate change, including potential adverse flood impacts and opportunities for replenishing water storages.~~

~~Second, in regions with enhanced mean precipitation , increasesin~~ Second, where mean precipitation also increases, larger RX5day ~~augment the blue water share. In these cases, soils may become saturated more frequently linked to increasing baseline rainfall (Fig. S9). Consequently, subsequent~~ changes can further enhance blue water shares because wetter mean conditions make saturation-driven runoff during extreme precipitation events ~~are more likelyto trigger flooding, further highlighting the challenges that larger blue water shares pose for water management. The dependence of~~ more likely. This helps explain why ΔRX5day ~~magnitudes on baseline precipitation stresses the importance of also considering average precipitation change (Fig. 3a ,b). This effect may particularly emerge in the blue water regime, where average precipitation is projected to increase in over 89% of the area, with a mean increase of 0.24 (~8 %) (~~emerges as the dominant positive predictor of ΔBGWS despite contrasting regional trends in mean precipitation.

The dominant role of ΔRX5day is consistent with studies showing strong effects of rainfall extremes on runoff ratios and catchment retention (Yang et al., 2018; Scheff et al., 2022). We extend this insight from retention and runoff-based metrics to a partitioning metric that also includes transpiration, linking precipitation intensity and plant water use to the balance between runoff and transpiration. Whereas Mankin et al. (2018) found that runoff partitioning changes are governed by precipitation changes, including mean precipitation and five-day precipitation extremes, our results identify extreme five-day precipitation as the leading spatial predictor of projected BGWS change.

The strongest negative predictor of the ensemble mean ΔBGWS field in both regimes is ΔLAI, which is strongly supported by the individual ESM results (Fig. 3). ~~Besides precipitation intensification, changes in LAI show a strong relationship with BGWS trends. ~~). Larger increases in LAI are associated with greener partitioning, indicating that vegetation expansion tends to favour transpiration relative to runoff. This provides the main counterweight to the positive RX5day effect and helps explain why blue-to-green shifts still occupy a substantial fraction of global land area despite the dominant blueward influence of extreme precipitation. Global greening is evident in the ensemble mean, with ~~LAI increases that are nearly twice as large in the~~ larger LAI increases in the historical blue water regime (Fig. ~~3c,d~~S9). Particularly blue water-dominated higher and mid-latitudes experience extensive vegetation growth due to global warming, where energy and temperature limitation is the primary controlling factor. ~~Besides~~In addition, CO_2 fertilisation and scenario-dependent land-use changes further impact LAI (Hurtt et al., 2020; Zhao et al., 2020). ~~The potential expansion in vegetation increases transpiration water demand, contributing to a larger green water share, as reflected by the strong negative regression coefficient. In addition, greater LAI elevates~~ Overall, larger LAI is associated with increased transpiration water demand and may also increase canopy interception losses, thereby reducing throughfall and runoff and potentially reinforcing green-ward shifts. ~~In the green~~

Beyond the two dominant predictors, the importance structure differs between the two historical regimes. In the blue water regime, ~~LAI changes have a similar positive effect on the green water share, but their importance to BGWS change is lower (Fig. 3b).~~

~~WUE is increasing in both regimes, likely due to rising CO_2 levels that affect stomatal conductance and GPP. The increase is smaller in blue water-dominated regions (Fig. 3c,d), which might be due to sufficient water availability in most blue water areas and plant-type-specific responses (Gentine et al., 2019). Yet, the latter processes are insufficiently captured in ESMs as plant functional types are limited in number and oversimplify ecological dynamics (Anderegg et al., 2022). WUE effects on BGWS trends are particularly strong in~~ ΔSM_{surf} is the third most important predictor in the ensemble mean, indicating that wetter near-surface soils favour larger blue water shares. This is consistent with the blue water regime being concentrated in already wet, energy-limited, or seasonally wet regions, where further increases in near-surface soil moisture help maintain or strengthen runoff-dominated partitioning by increasing the likelihood of saturation-driven runoff (Singh et al., 2021). In the green water regime~~(Fig. 3b). Here, the ensemble mean shows a decrease in mean transpiration, despite expanding vegetation (Fig. 3d). The suppressing effect of rising WUE on green water flow leads to an increase in the blue water share (Fig. 3b), consistent with the "plants-turn-on-the-tap" mechanism (Idso and Brazel, 1984). Consequently, WUE changes play a key role in blue water share increases within the green water regime (i.e., 30.9% of global land area with blue water share increases within the green water regime) and potentially drive the green-to-blue regime shift observed in 6.3% of the global land area (Tables S3 and S4)~~,~~ ΔVPD_{seas} is the third most important predictor in the ensemble mean, suggesting that stronger seasonal atmospheric dryness favours greener partitioning. This is consistent with the green water regime being concentrated in water-limited or strongly seasonal climates, where the seasonal contrast in atmospheric moisture demand remains an important control on transpiration-dominated partitioning (Seneviratne et al., 2010; Young et al., 2022). The exact ranking of lower-order predictors, however, is less stable and should not be overemphasised, because differences in ensemble-mean permutation importance are small and rankings also vary across individual ESMs. In summary, the predictor rankings suggest that projected BGWS changes arise primarily from the interplay between precipitation intensification and vegetation expansion, while plant–atmosphere controls on transpiration and changes in near-surface wetness emerge as additional regionally relevant predictors.

3.4 ~~Management implications~~ Implications of future BGWS trends

The BGWS metric is a process rather than a quantity indicator. It characterises how an incremental unit of precipitation (e.g., the next millimetre of rain) is partitioned between runoff (blue water) and plant use via transpiration (green water), not how large those fluxes are in absolute terms. In this sense, BGWS addresses the question "where does the next unit of rain tend to go?" rather than "how much water is there overall?". ~~This~~ As our analysis excludes hyper-arid and sparsely vegetated regions, this distinction matters for impacts that depend on hydrological sensitivity and timing (Nijssen et al., 2001)~~, such as runoff responsiveness (flashiness), baseflow sustainment, soil-moisture buffering, and canopy evaporative cooling, affecting both ecosystems and human water management, even when absolute amounts of precipitation, runoff, or transpiration rise or fall~~. It shifts the focus from one on absolute change, to one in which we try to understand controlling factors and enables

another level of model evaluation that centres on comparing these controlling factors rather than just focusing on matching historical observations (Wagener et al., 2022). Although our analysis is flow-based and excludes storage terms, persistent BGWS shifts signal sustained pressure on blue water stores (e.g., rivers, reservoirs, groundwater) versus green water stores (root-zone moisture).

BGWS changes become most meaningful ~~for management~~ when interpreted jointly with absolute ~~hydroecological changes rather than analysing partitioning shifts or absolute changes (e.g., RX5day) in isolation . This joint interpretation provides a more complete picture of blue and green water processes and their implications. For water management, combining BGWS changes with absolute changes in runoff yields decision-relevant insights~~ changes in runoff and transpiration rather than in isolation (Fig. 4). In combination with runoff changes (Fig. 4a~~; conceptual synthesis in Fig. 5). Where BGWS and runoff changes~~), the robust sign combinations point to four distinct hydrological implications. Where ΔBGWS and ΔR are both positive, ~~managers should anticipate~~ both runoff volume and the runoff share of precipitation increase, indicating stronger blue-water partitioning and greater potential for ~~flood pressure , which enhances channel erosion and nutrient flushing~~ high-flow pressure during wet periods (e.g., southern Asia); where ΔBGWS is positive but ~~runoff change~~ ΔR is negative, ~~absolute runoff shrinks yet vegetation water use declines even more strongly (e.g., western Mediterranean)~~runoff shrinks in absolute terms but its share of precipitation still increases. Thus, the relative contribution of runoff pathways per unit precipitation increases, ~~thereby raising the potential for intense runoff generation during extreme precipitation events. This aligns with catchment-scale evidence that rising precipitation intensity shifts precipitation partitioning toward fast runoff, erodes green water storage, and threatens reservoir reliability (Eekhout et al., 2018)~~indicating higher runoff sensitivity to intense rainfall. Yet, this pattern occurs only rarely in the robust map. Conversely, negative ΔBGWS with positive ~~runoff change~~ ΔR suggests more total runoff but a smaller ~~fraction per event, potentially improving baseflow support if soil moisture increases~~ share of precipitation, implying that runoff may remain elevated if water supply stays sufficient (e.g., ~~Eastern Canada); when both ΔBGWS and runoff changes~~ northwestern Eurasia); where both ΔBGWS and ΔR are negative, shrinking blue water volumes and shares indicate ~~water-scarcity and ecological-flow risks that call for demand management, soil-moisture conservation and increased storage~~ concurrent pressure on blue-water supply (e.g., ~~Amazon rainforest~~large parts of Europe). Comparable patterns are seen during European droughts, where blue water declines outpace green water responses, tightening low-flows even when vegetation maintains transpiration (Orth and Destouni, 2018).

~~For land-management, interpreting BGWS jointly with absolute changes in transpiration provides~~ Joint interpretation of BGWS with transpiration changes adds eco-physiological and land-surface insight (Fig. 4b~~; conceptual synthesis in Fig. S5~~). Where ~~BGWS and transpiration increase~~ΔBGWS and ΔE_t are both positive, landscapes become more runoff-dominated while plant water use rises, ~~signalling~~ consistent with higher atmospheric/phenological demand and greater reliance on stored water (e.g., ~~Horn of Africa~~northeastern Eurasia); where ~~BGWS increases but transpiration decreases~~ΔBGWS is positive and ΔE_t is negative, partitioning shifts toward runoff as vegetation down-regulates (e.g., ~~C. Australia~~southeastern South America). The latter response reduces evaporative cooling and elevates heat risk (He et al., 2022). Conversely, ~~BGWS decreases with transpiration increases indicate greater green water allocation and stronger latent cooling, supporting vegetation productivity and microclimate buffering, but they also signal faster soil-moisture depletion and rising irrigation demand when precipitation~~

decreases where ΔBGWS is negative and ΔE_t is positive, regions experience greener partitioning, which may strengthen land–atmosphere coupling and support stronger latent cooling (e.g., western northeastern North America); when both BGWS and transpiration ΔBGWS and ΔE_t decrease, relative allocation to green water rises despite lower plant water use, flagging which points to weaker evaporative cooling and habitat vegetation-mediated buffering of heat and moisture stress (e.g., parts of the Amazon rainforest).

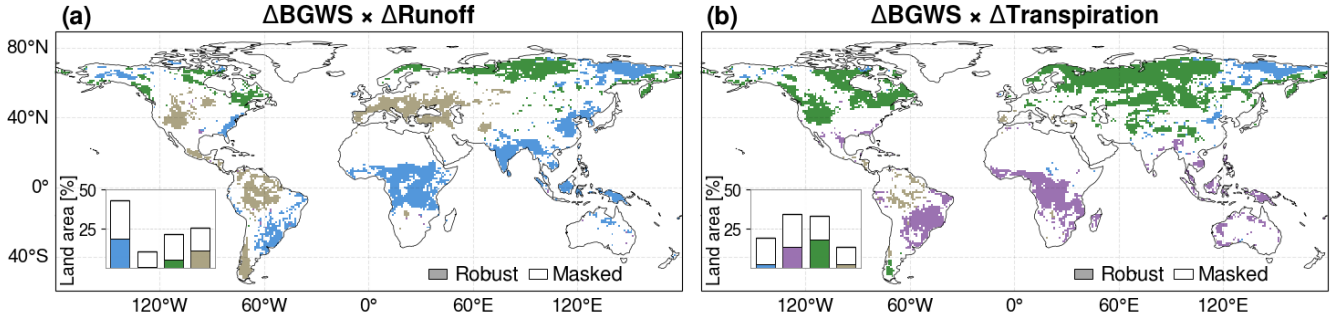

(c)	↑ Runoff	↓ Runoff	↑ Transpiration	↓ Transpiration
↑ BGWS	• Larger blue water share and more runoff • Stronger runoff response per unit precipitation • May increase flood pressure in high flow periods	• Larger blue water share and less runoff • Transpiration declines more than runoff • Suggests stronger runoff sensitivity to intense rainfall	• Larger blue water share and more transpiration • May reflect higher atmospheric or phenological demand • May raise blue water scarcity in dry periods	• Larger blue water share and less transpiration • Lower vegetation water use shifts partitioning toward runoff • May reduce evaporative cooling and increase heat stress
↓ BGWS	• Larger green water share and more runoff • Transpiration increases more strongly than runoff • Runoff may remain elevated where water supply is sufficient	• Larger green water share and less runoff • Points to lower blue water availability • May increase pressure on water supply	• Larger green water share and more transpiration • Reflects a stronger transpiration response • May strengthen land-atmosphere coupling	• Larger green water share and less transpiration • Could suggest limits on plant water use • May reduce evaporative cooling and vegetation buffering

Figure 4. Conceptual classification matrix illustrating the implications of joint projected Projected changes (2071–2100 minus 1985–2014) in the Blue-Green Water Share (BGWS) blue–green water partitioning and absolute associated runoff and transpiration responses. The matrix summarises the dominant hydrological Panels (a) andecological responses associated with (b) show the direction of joint ensemble -mean ΔBGWS combined with changes in BGWS runoff and absolute flows under SSP3-7.0transpiration, based on 11 CMIP6 ESMs. Coloured labels correspond respectively, for the end of the century relative to the historical period. Colours indicate the four quadrants of joint sign combinations between ΔBGWS and the corresponding flux change, as defined schematically in panel (blue = ΔBGWS ↑ & flow ↑; violet = ΔBGWS ↑ & flow ↓; green = ΔBGWS ↓ & flow ↑; brown = ΔBGWS ↓ & flow ↓c), which also summarises their possible hydroecological implications. White grid cells in panels (a) and (b) denote areas excluded by the historical analysis mask or masked because fewer than 8 of the 12 models agree on the same joint quadrant class. Insets show the land-area fraction of each quadrant class, with coloured bar segments indicating robust area and white segments indicating area masked because of low agreement.

In communicating results, ~~uncertainty is decision-relevant and should be made explicit. In blue water regimes, spatial means indicate both larger responses and larger inter-model spread in hydrological variables and vegetation metrics, whereas in green water regimes the mean hydrological response is more certain but the spread in transpiration remains comparably large (~~it is important to make uncertainty explicit. Fig. ~~3c,d). Our maps further show that sizeable areas do not reach $\geq 70\,\%$ ensemble agreement (i.e. fewer than 8 of 11 models), signalling sign-uncertain changeat the grid-cell scale (Figs. 2, 4 and S9). Water and land management should therefore distinguish sign-robust patterns, which justify no-regrets measures consistent with the implied risk pathway, from magnitude- or sign-uncertain patterns, which call for adaptive pathways, flexible design ranges, and enhanced monitoring~~4 therefore only shows areas where at least eight of the twelve models agree on the sign of both ΔBGWS and the corresponding flux change. Even so, the results should be read as robust regional tendencies rather than local predictions. In regions with robust sign agreement, joint interpretation of ΔBGWS with ΔR and ΔE_t provides a compact way to distinguish whether future change is more likely to intensify runoff sensitivity, strengthen transpiration demand, or simultaneously reduce water availability and vegetation cooling. Given the additional baseline biases relative to reanalysis and observation-based products (~~Figs.S1, S3 and S4~~Sect. S3), a regionalised and observationally constrained analysis of ΔBGWS and co-varying hydroecological responses ~~could yield actionable, sector-specific insights for water allocation, flood protection, irrigation demand, environmental flows, and heat mitigation~~would still be needed before drawing site-specific management conclusions.

~~4 Discussion and conclusion~~

4 Conclusions

~~The introduction of the BGWS brings several advances in quantifying and understanding precipitation partitioning between blue and green water , and its combination with absolute changes in hydroecological variables yields impact-relevant insights.~~ In this study, we assessed where future blue–green water partitioning shifts favour blue or green water pathways and which climatic and hydroecological changes are associated with these shifts. To do so, we defined the BGWS and applied it to 12 CMIP6 ESMs under SSP3–7.0, focusing on vegetated and hydrologically active land areas. Together, the results show distinct historical partitioning regimes, spatially heterogeneous future shifts, and a dominant role of precipitation intensification that is partly counteracted by vegetation expansion.

~~Our finding that extreme precipitation changes have the largest impact on partitioning shifts aligns with studies showing strong effects of rainfall extremes on runoff ratios and catchment retention (Yang et al., 2018; Scheff et al., 2022). We extend this insight from retention and runoff volumes to an explicit partitioning metric that includes transpiration. This links precipitation intensity and plant physiology to how precipitation is partitioned between channel flow and plant use. Separating historical blue and green regimesclarifies offsetting effects that can mask net global signals in runoff ratios. We also concur with Yang et al. (Yang et al., 2018) that explicitly quantifying intra-annual hydroclimate variability would enhance understanding in highly seasonal climates. We extend this recommendation to precipitation-partitioning dynamics.~~

Relative to the blue water trade-off (BWT) metric used by Mankin et al. (Mankin et al., 2018, 2019), the BGWS contrasts runoff directly with transpiration, excluding interception or storage, and reports it as a normalised share of precipitation Historically, BGWS separates cold, high-altitude, and strongly seasonal regions with larger blue water shares from many water-limited regions with larger green water shares. Future changes show a slight ensemble-mean shift towards larger blue water shares, with strengthening or weakening of existing regimes more common than full regime shifts. Thus, interception-driven canopy effects are not represented explicitly by the BGWS . For assessing green water, however, transpiration as a direct ESM output is beneficial and more readily translated to land-management perspectives as the immediate indicator of plant water use. In contrast to Mankin et al. (Mankin et al., 2018), who found that increased blue water partitioning arises primarily from mean-precipitation increases reinforced by extremes, we show that extreme The main predictor of projected BGWS change is increasing extreme five-day precipitation is the dominant driver of partitioning change. This is apparent across both historical regimes and independent of baseline precipitation. Considering BGWS alongside absolute changes in runoff and transpiration provides a compact interpretation that moves beyond quantifying partitioning shiftsand connects them to potential impacts on communities and ecosystems.

Together, these advances position BGWS as a simple, interpretable metric that isolates the runoff–transpiration pathway, elevates RX5day as the leading global driver, identifies LAI and WUE as secondary regime-dependent controls, and, when paired precipitation, which favours larger blue water shares, while increasing LAI provides the main counterweight by favouring vegetation-mediated green water use. Interpreting BGWS together with absolute runoff and transpiration changes , translates partitioning shifts into decision-relevant guidance. BGWS complements, rather than replaces, canopy-focused trade-off and retention metricshelps distinguish where future changes may increase runoff sensitivity, strengthen vegetation water use, reduce blue water availability, or weaken vegetation-mediated cooling.

Nonetheless, uncertainties and biases in ESM studies remain since because BGWS dynamics depend on the representation of hydroclimatic and biogeochemical processes (Clark et al., 2015; Gentine et al., 2019; Zheng et al., 2019; Padrón et al., 2022; Yang et al., 2023; Gier et al., 2024). An additional source of uncertainty is that many large-scale land models used in ESMs still represent lateral groundwater redistribution only in a limited or highly simplified way, partly because coarse model resolution does not resolve subgrid land-surface heterogeneity well (Liao et al., 2025). This can affect blue–green water partitioning by underrepresenting shallow groundwater support to ET during dry periods, potentially favouring a more blue-biased partitioning (Maxwell and Condon, 2016).

Despite these uncertainties, particularly in the land-surface components and their assumptions regarding plant responses to elevated CO_2, robust signals of BGWS shifts emerge. Yet, within the ESM ensemble emerge. While we used LAI as a proxy for vegetation responses that reflect both climatic and human influences, future research could assess land-use and land-cover changes more explicitly. Additionally, advancing both observational data and ESMs appears vital to improve the reliability of future projections on terrestrial freshwater availability, including a more consistent treatment of human influences such as irrigation. Coupling these advancements with process-based ESM evaluations will can deepen insights into blue--green water partitioning and vegetation-climate feedbacks , paving the way for more robust and actionable vegetation–climate feedbacks and support more robust climate information, especially in understudied, high-impact regions (Stein et al., 2024).

Code and data availability. The CMIP6 datasets used in this study were accessed through the Deutsche Klimarechenzentrum (DKRZ) CMIP Data Pool (last access: 20 June 2025) and the Earth System Grid Federation (https://aims2.llnl.gov) portal. The DKRZ CMIP Data Pool (available at https://cmip-data-pool.dkrz.de) is restricted to registered users with a valid DKRZ account. The GPCC monthly product is available for download from DWD Open Data: https://opendata.dwd.de/climate_environment /GPCC/html/fulldata-monthly_v2022_doi_download.html (last access: 10 January 2025). The G-RUN dataset is publicly available at Figshare: https://figshare.com/articles/dataset/G-RUN_ENSEMBLE /12794075 (last access: 10 January 2025). The GLEAM dataset is available via SFTP (Secure File Transfer Protocol) and requires user registration for access. Credentials can be requested at GLEAM website: https://www.gleam.eu (last access: 10 January 2025). ERA5-Land data is publicly available through the Copernicus CDS (last access: 10 January 2025). All code to reproduce this analysis is publicly available on GitHub at: https://github.com/simonheselschwerdt/bgws_analysis.

Author contributions. S.P.H. and P.G. conceived the study and designed the analysis. S.P.H. conducted the analysis and led the writing of the manuscript. All authors discussed the methods and results and contributed to writing and edited the manuscript.

Competing interests. Some authors are members of the editorial board of Earth System Dynamics.

Acknowledgements. This study is financially supported by the Helmholtz Association Initiative and Networking Fund (IVF). We acknowledge the World Climate Research Programme's Working Group on Coupled Modelling, which is responsible for CMIP, and we thank the climate modelling groups for producing and making available their model output. This work used resources of the Deutsches Klimarechenzentrum (DKRZ, https://www.dkrz.de) granted by its Scientific Steering Committee (WLA) under project ID ch0636. S.P.H. and P.G. also thank Peter Hoffmann for internally reviewing our paper draft. T.W. acknowledges support from the Alexander von Humboldt Foundation in the framework of the Alexander von Humboldt Professorship endowed by the German Federal Ministry of Education and Research (BMBF). L.W.-E. acknowledges financial support from Formas - a Swedish Research Council for Sustainable Development (2022-02089, 2023-00310, 2023-00321).

References

Althoff, D. and Destouni, G.: Global patterns in water flux partitioning: Irrigated and rainfed agriculture drives asymmetrical flux to vegetation over runoff, One Earth, 6, 1246–1257, https://doi.org/10.1016/j.oneear.2023.08.002, 2023.

Anderegg, L. D. L., Griffith, D. M., Cavender-Bares, J., Riley, W. J., Berry, J. A., Dawson, T. E., and Still, C. J.: Representing plant diversity in land models: An evolutionary approach to make "Functional Types" more functional, Global Change Biology, 28, 2541–2554, https://doi.org/10.1111/gcb.16040, 2022.

Barnett, T. P., Adam, J. C., and Lettenmaier, D. P.: Potential impacts of a warming climate on water availability in snow-dominated regions, Nature, 438, 303–309, https://doi.org/10.1038/nature04141, 2005.

Berg, A. and Sheffield, J.: Evapotranspiration Partitioning in CMIP5 Models: Uncertainties and Future Projections, Journal of Climate, 32, 2653–2671, https://doi.org/10.1175/JCLI-D-18-0583.1, 2019.

Betts, R. A., Cox, P. M., Collins, M., Harris, P. P., Huntingford, C., and Jones, C. D.: The role of ecosystem-atmosphere interactions in simulated Amazonian precipitation decrease and forest dieback under global climate warming, Theoretical and Applied Climatology, 78, 157–175, https://doi.org/10.1007/s00704-004-0050-y, 2004.

Betts, R. A., Boucher, O., Collins, M., Cox, P. M., Falloon, P. D., Gedney, N., Hemming, D. L., Huntingford, C., Jones, C. D., Sexton, D. M. H., and Webb, M. J.: Projected increase in continental runoff due to plant responses to increasing carbon dioxide, Nature, 448, 1037–1041, https://doi.org/10.1038/nature06045, 2007.

Bouaziz, L. J. E., Aalbers, E. E., Weerts, A. H., Hegnauer, M., Buiteveld, H., Lammersen, R., Stam, J., Sprokkereef, E., Savenije, H. H. G., and Hrachowitz, M.: Ecosystem adaptation to climate change: the sensitivity of hydrological predictions to time-dynamic model parameters, Hydrology and Earth System Sciences, 26, 1295–1318, https://doi.org/10.5194/hess-26-1295-2022, 2022.

Boucher, O., Servonnat, J., Albright, A. L., Aumont, O., Balkanski, Y., Bastrikov, V., Bekki, S., Bonnet, R., Bony, S., Bopp, L., Braconnot, P., Brockmann, P., Cadule, P., Caubel, A., Cheruy, F., Codron, F., Cozic, A., Cugnet, D., D'Andrea, F., Davini, P., de Lavergne, C., Denvil, S., Deshayes, J., Devilliers, M., Ducharne, A., Dufresne, J.-L., Dupont, E., Éthé, C., Fairhead, L., Falletti, L., Flavoni, S., Foujols, M.-A., Gardoll, S., Gastineau, G., Ghattas, J., Grandpeix, J.-Y., Guenet, B., Guez, Lionel, E., Guilyardi, E., Guimberteau, M., Hauglustaine, D., Hourdin, F., Idelkadi, A., Joussaume, S., Kageyama, M., Khodri, M., Krinner, G., Lebas, N., Levavasseur, G., Lévy, C., Li, L., Lott, F., Lurton, T., Luyssaert, S., Madec, G., Madeleine, J.-B., Maignan, F., Marchand, M., Marti, O., Mellul, L., Meurdesoif, Y., Mignot, J., Musat, I., Ottlé, C., Peylin, P., Planton, Y., Polcher, J., Rio, C., Rochetin, N., Rousset, C., Sepulchre, P., Sima, A., Swingedouw, D., Thiéblemont, R., Traore, A. K., Vancoppenolle, M., Vial, J., Vialard, J., Viovy, N., and Vuichard, N.: Presentation and Evaluation of the IPSL-CM6A-LR Climate Model, Journal of Advances in Modeling Earth Systems, 12, e2019MS002 010, https://doi.org/10.1029/2019MS002010, 2020.

Breiman, L.: Random Forests, Machine Learning, 45, 5–32, https://doi.org/10.1023/A:1010933404324, 2001.

Brunner, L., Poschlod, B., Dutra, E., Fischer, E. M., Martius, O., and Sillmann, J.: A global perspective on the spatial representation of climate extremes from km-scale models, Environmental Research Letters, 20, 074 054, https://doi.org/10.1088/1748-9326/ade1ef, 2025.

Buck, A. L.: New Equations for Computing Vapor Pressure and Enhancement Factor, Journal of Applied Meteorology and Climatology, 20, 1527–1532, https://doi.org/10.1175/1520-0450(1981)020<1527:NEFCVP>2.0.CO;2, 1981.

Budyko, M. I.: Climate and Life, Academic Press, New York, 1974.

Clark, M. P., Fan, Y., Lawrence, D. M., Adam, J. C., Bolster, D., Gochis, D. J., Hooper, R. P., Kumar, M., Leung, L. R., Mackay, D. S., Maxwell, R. M., Shen, C., Swenson, S. C., and Zeng, X.: Improving the representation of hydrologic processes in Earth System Models, Water Resources Research, 51, 5929–5956, https://doi.org/10.1002/2015WR017096, 2015.

Danabasoglu, G., Lamarque, J.-F., Bacmeister, J., Bailey, D. A., DuVivier, A. K., Edwards, J., Emmons, L. K., Fasullo, J., Garcia, R., Gettelman, A., Hannay, C., Holland, M. M., Large, W. G., Lauritzen, P. H., Lawrence, D. M., Lenaerts, J. T. M., Lindsay, K., Lipscomb, W. H., Mills, M. J., Neale, R., Oleson, K. W., Otto-Bliesner, B., Phillips, A. S., Sacks, W., Tilmes, S., van Kampenhout, L., Vertenstein, M., Bertini, A., Dennis, J., Deser, C., Fischer, C., Fox-Kemper, B., Kay, J. E., Kinnison, D., Kushner, P. J., Larson, V. E., Long, M. C., Mickelson, S., Moore, J. K., Nienhouse, E., Polvani, L., Rasch, P. J., and Strand, W. G.: The Community Earth System Model Version 2 (CESM2), Journal of Advances in Modeling Earth Systems, 12, e2019MS001 916, https://doi.org/10.1029/2019MS001916, 2020.

Denissen, J. M. C., Teuling, A. J., Pitman, A. J., Koirala, S., Migliavacca, M., Li, W., Reichstein, M., Winkler, A. J., Zhan, C., and Orth, R.: Widespread shift from ecosystem energy to water limitation with climate change, Nature Climate Change, 12, 677–684, https://www.nature.com/articles/s41558-022-01403-8, 2022.

Donat, M. G., Lowry, A. L., Alexander, L. V., O'Gorman, P. A., and Maher, N.: More extreme precipitation in the world's dry and wet regions, Nature Climate Change, 6, 508–513, https://doi.org/10.1038/nclimate2941, 2016.

Dunn, R. J. H., Donat, M. G., and Alexander, L. V.: Comparing extremes indices in recent observational and reanalysis products, Frontiers in Climate, 4, https://doi.org/10.3389/fclim.2022.989505, 2022.

Dunne, J. P., Horowitz, L. W., Adcroft, A. J., Ginoux, P., Held, I. M., John, J. G., Krasting, J. P., Malyshev, S., Naik, V., Paulot, F., Shevliakova, E., Stock, C. A., Zadeh, N., Balaji, V., Blanton, C., Dunne, K. A., Dupuis, C., Durachta, J., Dussin, R., Gauthier, P. P. G., Griffies, S. M., Guo, H., Hallberg, R. W., Harrison, M., He, J., Hurlin, W., McHugh, C., Menzel, R., Milly, P. C. D., Nikonov, S., Paynter, D. J., Ploshay, J., Radhakrishnan, A., Rand, K., Reichl, B. G., Robinson, T., Schwarzkopf, D. M., Sentman, L. T., Underwood, S., Vahlenkamp, H., Winton, M., Wittenberg, A. T., Wyman, B., Zeng, Y., and Zhao, M.: The GFDL Earth System Model Version 4.1 (GFDL-ESM 4.1): Overall Coupled Model Description and Simulation Characteristics, Journal of Advances in Modeling Earth Systems, 12, e2019MS002 015, https://doi.org/10.1029/2019MS002015, _eprint: https://onlinelibrary.wiley.com/doi/pdf/10.1029/2019MS002015, 2020.

Dunne, T. and Black, R. D.: An Experimental Investigation of Runoff Production in Permeable Soils, Water Resources Research, 6, 478–490, https://doi.org/10.1029/WR006i002p00478, 1970.

Dutta, R. and Markonis, Y.: Does ERA5-land capture the changes in the terrestrial hydrological cycle across the globe?, Environmental Research Letters, 19, 024 054, https://doi.org/10.1088/1748-9326/ad1d3a, 2024.

Döscher, R., Acosta, M., Alessandri, A., Anthoni, P., Arsouze, T., Bergman, T., Bernardello, R., Boussetta, S., Caron, L.-P., Carver, G., Castrillo, M., Catalano, F., Cvijanovic, I., Davini, P., Dekker, E., Doblas-Reyes, F. J., Docquier, D., Echevarria, P., Fladrich, U., Fuentes-Franco, R., Gröger, M., v. Hardenberg, J., Hieronymus, J., Karami, M. P., Keskinen, J.-P., Koenigk, T., Makkonen, R., Massonnet, F., Ménégoz, M., Miller, P. A., Moreno-Chamarro, E., Nieradzik, L., van Noije, T., Nolan, P., O'Donnell, D., Ollinaho, P., van den Oord, G., Ortega, P., Prims, O. T., Ramos, A., Reerink, T., Rousset, C., Ruprich-Robert, Y., Le Sager, P., Schmith, T., Schrödner, R., Serva, F., Sicardi, V., Sloth Madsen, M., Smith, B., Tian, T., Tourigny, E., Uotila, P., Vancoppenolle, M., Wang, S., Wårlind, D., Willén, U., Wyser, K., Yang, S., Yepes-Arbós, X., and Zhang, Q.: The EC-Earth3 Earth system model for the Coupled Model Intercomparison Project 6, Geoscientific Model Development, 15, 2973–3020, https://doi.org/10.5194/gmd-15-2973-2022, 2022.

Eekhout, J. P. C., Hunink, J. E., Terink, W., and de Vente, J.: Why increased extreme precipitation under climate change negatively affects water security, Hydrology and Earth System Sciences, 22, 5935–5946, https://doi.org/10.5194/hess-22-5935-2018, 2018.

Eyring, V., Bony, S., Meehl, G. A., Senior, C. A., Stevens, B., Stouffer, R. J., and Taylor, K. E.: Overview of the Coupled Model Intercomparison Project Phase 6 (CMIP6) experimental design and organization, Geoscientific Model Development, 9, 1937–1958, https://doi.org/10.5194/gmd-9-1937-2016, 2016.

Falkenmark, M.: Land–water linkages: a synopsis, in: Land and Water Integration and River Basin Management, Proceedings of the FAO Workshop, Rome, 31 January–2 February 1993, pp. 15–17, FAO, Rome, https://www.fao.org/4/v5400e/v5400e00.htm, 1995.

Falkenmark, M.: Growing water scarcity in agriculture: future challenge to global water security, Philosophical Transactions of the Royal Society A: Mathematical, Physical and Engineering Sciences, 371, 20120 410, https://doi.org/10.1098/rsta.2012.0410, 2013.

Falkenmark, M. and Rockström, J.: The New Blue and Green Water Paradigm: Breaking New Ground for Water Resources Planning and Management, Journal of Water Resources Planning and Management, 132, 129–132, https://doi.org/10.1061/(ASCE)0733-9496(2006)132:3(129), 2006.

Falkenmark, M. and Rockström, J.: Building Water Resilience in the Face of Global Change: From a Blue-Only to a Green-Blue Water Approach to Land-Water Management, Journal of Water Resources Planning and Management, 136, 606–610, https://doi.org/10.1061/(ASCE)WR.1943-5452.0000118, 2010.

Falkenmark, M., Wang-Erlandsson, L., and Rockström, J.: Understanding of water resilience in the Anthropocene, Journal of Hydrology X, 2, 100 009, https://doi.org/10.1016/j.hydroa.2018.100009, 2019.

Fiedler, S., Crueger, T., D'Agostino, R., Peters, K., Becker, T., Leutwyler, D., Paccini, L., Burdanowitz, J., Buehler, S. A., Cortes, A. U., Dauhut, T., Dommenget, D., Fraedrich, K., Jungandreas, L., Maher, N., Naumann, A. K., Rugenstein, M., Sakradzija, M., Schmidt, H., Sielmann, F., Stephan, C., Timmreck, C., Zhu, X., and Stevens, B.: Simulated Tropical Precipitation Assessed across Three Major Phases of the Coupled Model Intercomparison Project (CMIP), Monthly Weather Review, 148, 3653–3680, https://doi.org/10.1175/MWR-D-19-0404.1, 2020.

Forzieri, G., Miralles, D. G., Ciais, P., Alkama, R., Ryu, Y., Duveiller, G., Zhang, K., Robertson, E., Kautz, M., Martens, B., Jiang, C., Arneth, A., Georgievski, G., Li, W., Ceccherini, G., Anthoni, P., Lawrence, P., Wiltshire, A., Pongratz, J., Piao, S., Sitch, S., Goll, D. S., Arora, V. K., Lienert, S., Lombardozzi, D., Kato, E., Nabel, J. E. M. S., Tian, H., Friedlingstein, P., and Cescatti, A.: Increased control of vegetation on global terrestrial energy fluxes, Nature Climate Change, 10, 356–362, https://doi.org/10.1038/s41558-020-0717-0, 2020.

Fowler, M. D., Kooperman, G. J., Randerson, J. T., and Pritchard, M. S.: The effect of plant physiological responses to rising CO2 on global streamflow, Nature Climate Change, 9, 873–879, https://doi.org/10.1038/s41558-019-0602-x, 2019.

Friedman, J. H., Hastie, T., and Tibshirani, R.: Regularization Paths for Generalized Linear Models via Coordinate Descent, Journal of Statistical Software, 33, 1–22, https://doi.org/10.18637/jss.v033.i01, 2010.

Fujimori, S., Hasegawa, T., Masui, T., Takahashi, K., Herran, D. S., Dai, H., Hijioka, Y., and Kainuma, M.: SSP3: AIM implementation of Shared Socioeconomic Pathways, Global Environmental Change, 42, 268–283, https://doi.org/10.1016/j.gloenvcha.2016.06.009, 2017.

Gedney, N., Huntingford, C., Weedon, G. P., Bellouin, N., Boucher, O., and Cox, P. M.: Detection of solar dimming and brightening effects on Northern Hemisphere river flow, Nature Geoscience, 7, 796–800, https://doi.org/10.1038/ngeo2263, 2014.

Gentine, P., Green, J. K., Guérin, M., Humphrey, V., Seneviratne, S. I., Zhang, Y., and Zhou, S.: Coupling between the terrestrial carbon and water cycles—a review, Environmental Research Letters, 14, 083 003, https://doi.org/10.1088/1748-9326/ab22d6, 2019.

Ghiggi, G., Humphrey, V., Seneviratne, S. I., and Gudmundsson, L.: GRUN: an observation-based global gridded runoff dataset from 1902 to 2014, Earth System Science Data, 11, 1655–1674, https://doi.org/10.5194/essd-11-1655-2019, 2019.

Gier, B. K., Schlund, M., Friedlingstein, P., Jones, C. D., Jones, C., Zaehle, S., and Eyring, V.: Representation of the terrestrial carbon cycle in CMIP6, Biogeosciences, 21, 5321–5360, https://doi.org/10.5194/bg-21-5321-2024, 2024.

Gleeson, T., Wang-Erlandsson, L., Porkka, M., Zipper, S. C., Jaramillo, F., Gerten, D., Fetzer, I., Cornell, S. E., Piemontese, L., Gordon, L. J., Rockström, J., Oki, T., Sivapalan, M., Wada, Y., Brauman, K. A., Flörke, M., Bierkens, M. F. P., Lehner, B., Keys, P., Kummu, M., Wagener, T., Dadson, S., Troy, T. J., Steffen, W., Falkenmark, M., and Famiglietti, J. S.: Illuminating water cycle modifications and

Earth system resilience in the Anthropocene, Water Resources Research, 56, e2019WR024 957, https://doi.org/10.1029/2019WR024957, 2020a.

Gleeson, T., Wang-Erlandsson, L., Zipper, S. C., Porkka, M., Jaramillo, F., Gerten, D., Fetzer, I., Cornell, S. E., Piemontese, L., Gordon, L. J., Rockström, J., Oki, T., Sivapalan, M., Wada, Y., Brauman, K. A., Flörke, M., Bierkens, M. F. P., Lehner, B., Keys, P., Kummu, M., Wagener, T., Dadson, S., Troy, T. J., Steffen, W., Falkenmark, M., and Famiglietti, J. S.: The Water Planetary Boundary: Interrogation and Revision, One Earth, 2, 223–234, https://doi.org/10.1016/j.oneear.2020.02.009, 2020b.

Gnann, S., Baldwin, J. W., Cuthbert, M. O., Gleeson, T., Schwanghart, W., and Wagener, T.: The Influence of Topography on the Global Terrestrial Water Cycle, Reviews of Geophysics, 63, e2023RG000 810, https://doi.org/10.1029/2023RG000810, 2025.

Greve, P., Orlowsky, B., Mueller, B., Sheffield, J., Reichstein, M., and Seneviratne, S. I.: Global assessment of trends in wetting and drying over land, Nature Geoscience, 7, 716–721, https://doi.org/10.1038/ngeo2247, 2014.

Gudmundsson, L., Brunner, M. I., Döll, P., Fluet-Chouinard, E., Frolova, N., Gosling, S. N., Hirabayashi, Y., Kireeva, M. B., Liu, X., Müller Schmied, H., Magritskiy, D., Slater, L. J., Stein, L., Tramblay, Y., Wang, K., Wasko, C., Yamazaki, D., and Zhou, X.: Past and future change in global river flows, Nature Reviews Earth & Environment, 7, 7–23, https://doi.org/10.1038/s43017-025-00745-z, 2026.

Hajima, T., Watanabe, M., Yamamoto, A., Tatebe, H., Noguchi, M. A., Abe, M., Ohgaito, R., Ito, A., Yamazaki, D., Okajima, H., Ito, A., Takata, K., Ogochi, K., Watanabe, S., and Kawamiya, M.: Development of the MIROC-ES2L Earth system model and the evaluation of biogeochemical processes and feedbacks, Geoscientific Model Development, 13, 2197–2244, https://doi.org/10.5194/gmd-13-2197-2020, 2020.

Han, J., Yang, Y., Roderick, M. L., McVicar, T. R., Yang, D., Zhang, S., and Beck, H. E.: Assessing the Steady-State Assumption in Water Balance Calculation Across Global Catchments, Water Resources Research, 56, e2020WR027 392, https://doi.org/10.1029/2020WR027392, 2020.

Hausfather, Z. and Peters, G. P.: Emissions – the 'business as usual' story is misleading, Nature, 577, 618–620, https://doi.org/10.1038/d41586-020-00177-3, 2020.

He, M., Piao, S., Huntingford, C., Xu, H., Wang, X., Bastos, A., Cui, J., and Gasser, T.: Amplified warming from physiological responses to carbon dioxide reduces the potential of vegetation for climate change mitigation, Communications Earth & Environment, 3, 160, https://doi.org/10.1038/s43247-022-00489-4, 2022.

Horton, R. E.: The Role of infiltration in the hydrologic cycle, Eos, Transactions American Geophysical Union, 14, 446–460, https://doi.org/10.1029/TR014i001p00446, 1933.

Hou, Y., Guo, H., Yang, Y., and Liu, W.: Global Evaluation of Runoff Simulation From Climate, Hydrological and Land Surface Models, Water Resources Research, 59, e2021WR031 817, https://doi.org/10.1029/2021WR031817, 2023.

Huang, H., Liu, J., Chen, A., Ruiz-Vásquez, M., and Orth, R.: State-of-the-art hydrological datasets exhibit low water balance consistency globally, Earth System Science Data Discussions, pp. 1–23, https://doi.org/10.5194/essd-2025-376, 2025.

Hurtt, G. C., Chini, L., Sahajpal, R., Frolking, S., Bodirsky, B. L., Calvin, K., Doelman, J. C., Fisk, J., Fujimori, S., Klein Goldewijk, K., Hasegawa, T., Havlik, P., Heinimann, A., Humpenöder, F., Jungclaus, J., Kaplan, J. O., Kennedy, J., Krisztin, T., Lawrence, D., Lawrence, P., Ma, L., Mertz, O., Pongratz, J., Popp, A., Poulter, B., Riahi, K., Shevliakova, E., Stehfest, E., Thornton, P., Tubiello, F. N., van Vuuren, D. P., and Zhang, X.: Harmonization of global land use change and management for the period 850–2100 (LUH2) for CMIP6, Geoscientific Model Development, 13, 5425–5464, https://doi.org/10.5194/gmd-13-5425-2020, 2020.

Idso, S. B. and Brazel, A. J.: Rising atmospheric carbon dioxide concentrations may increase streamflow, Nature, 312, 51–53, https://doi.org/10.1038/312051a0, 1984.

Keenan, T. F., Hollinger, D. Y., Bohrer, G., Dragoni, D., Munger, J. W., Schmid, H. P., and Richardson, A. D.: Increase in forest water-use efficiency as atmospheric carbon dioxide concentrations rise, Nature, 499, 324–327, https://doi.org/10.1038/nature12291, 2013.

Knoben, W. J. M., Woods, R. A., and Freer, J. E.: A Quantitative Hydrological Climate Classification Evaluated With Independent Streamflow Data, Water Resources Research, 54, 5088–5109, https://doi.org/10.1029/2018WR022913, 2018.

Knutti, R., Furrer, R., Tebaldi, C., Cermak, J., and Meehl, G. A.: Challenges in Combining Projections from Multiple Climate Models, Journal of Climate, 23, 2739–2758, https://doi.org/10.1175/2009JCLI3361.1, 2010.

Laimighofer, J., Melcher, M., and Laaha, G.: Parsimonious statistical learning models for low-flow estimation, Hydrology and Earth System Sciences, 26, 129–148, https://doi.org/10.5194/hess-26-129-2022, 2022.

Lawrence, D. M., Thornton, P. E., Oleson, K. W., and Bonan, G. B.: The Partitioning of Evapotranspiration into Transpiration, Soil Evaporation, and Canopy Evaporation in a GCM: Impacts on Land–Atmosphere Interaction, Journal of Hydrometeorology, 8, 862–880, https://doi.org/10.1175/JHM596.1, 2007.

Leakey, A. D. B., Ainsworth, E. A., Bernacchi, C. J., Rogers, A., Long, S. P., and Ort, D. R.: Elevated CO2 effects on plant carbon, nitrogen, and water relations: six important lessons from FACE, Journal of Experimental Botany, 60, 2859–2876, https://doi.org/10.1093/jxb/erp096, 2009.

Lee, J.-E., Lintner, B. R., Neelin, J. D., Jiang, X., Gentine, P., Boyce, C. K., Fisher, J. B., Perron, J. T., Kubar, T. L., Lee, J., and Worden, J.: Reduction of tropical land region precipitation variability via transpiration, Geophysical Research Letters, 39, https://doi.org/10.1029/2012GL053417, 2012.

Li, C., Zwiers, F., Zhang, X., Li, G., Sun, Y., and Wehner, M.: Changes in Annual Extremes of Daily Temperature and Precipitation in CMIP6 Models, Journal of Climate, 34, 3441–3460, https://doi.org/10.1175/JCLI-D-19-1013.1, 2021a.

Li, J., Miao, C., Wei, W., Zhang, G., Hua, L., Chen, Y., and Wang, X.: Evaluation of CMIP6 Global Climate Models for Simulating Land Surface Energy and Water Fluxes During 1979–2014, Journal of Advances in Modeling Earth Systems, 13, e2021MS002 515, https://doi.org/10.1029/2021MS002515, 2021b.

Lian, X., Piao, S., Chen, A., Huntingford, C., Fu, B., Li, L. Z. X., Huang, J., Sheffield, J., Berg, A. M., Keenan, T. F., McVicar, T. R., Wada, Y., Wang, X., Wang, T., Yang, Y., and Roderick, M. L.: Multifaceted characteristics of dryland aridity changes in a warming world, Nature Reviews Earth & Environment, 2, 232–250, https://doi.org/10.1038/s43017-021-00144-0, 2021.

Liao, C., Leung, L. R., Fang, Y., Tesfa, T., and Negron-Juarez, R.: Representing lateral groundwater flow from land to river in Earth system models, Geoscientific Model Development, 18, 4601–4624, https://doi.org/10.5194/gmd-18-4601-2025, 2025.

Lovato, T., Peano, D., Butenschön, M., Materia, S., Iovino, D., Scoccimarro, E., Fogli, P. G., Cherchi, A., Bellucci, A., Gualdi, S., Masina, S., and Navarra, A.: CMIP6 Simulations With the CMCC Earth System Model (CMCC-ESM2), Journal of Advances in Modeling Earth Systems, 14, e2021MS002 814, https://doi.org/10.1029/2021MS002814, _eprint: https://agupubs.onlinelibrary.wiley.com/doi/pdf/10.1029/2021MS002814, 2022.

Lundberg, S. M. and Lee, S.-I.: A Unified Approach to Interpreting Model Predictions, Advances in Neural Information Processing Systems, 30, https://doi.org/10.48550/arXiv.1705.07874, 2017.

Mankin, J. S., Smerdon, J. E., Cook, B. I., Williams, A. P., and Seager, R.: The Curious Case of Projected Twenty-First-Century Drying but Greening in the American West, Journal of Climate, 30, 8689–8710, https://doi.org/10.1175/JCLI-D-17-0213.1, 2017.

Mankin, J. S., Seager, R., Smerdon, J. E., Cook, B. I., Williams, A. P., and Horton, R. M.: Blue Water Trade-Offs With Vegetation in a CO2-Enriched Climate, Geophysical Research Letters, 45, 3115–3125, https://doi.org/10.1002/2018GL077051, 2018.

Mankin, J. S., Seager, R., Smerdon, J. E., Cook, B. I., and Williams, A. P.: Mid-latitude freshwater availability reduced by projected vegetation responses to climate change, Nature Geoscience, 12, 983–988, https://doi.org/10.1038/s41561-019-0480-x, 2019.

Mauritsen, T., Bader, J., Becker, T., Behrens, J., Bittner, M., Brokopf, R., Brovkin, V., Claussen, M., Crueger, T., Esch, M., Fast, I., Fiedler, S., Fläschner, D., Gayler, V., Giorgetta, M., Goll, D. S., Haak, H., Hagemann, S., Hedemann, C., Hohenegger, C., Ilyina, T., Jahns, T., Jimenéz-de-la Cuesta, D., Jungclaus, J., Kleinen, T., Kloster, S., Kracher, D., Kinne, S., Kleberg, D., Lasslop, G., Kornblueh, L., Marotzke, J., Matei, D., Meraner, K., Mikolajewicz, U., Modali, K., Möbis, B., Müller, W. A., Nabel, J. E. M. S., Nam, C. C. W., Notz, D., Nyawira, S.-S., Paulsen, H., Peters, K., Pincus, R., Pohlmann, H., Pongratz, J., Popp, M., Raddatz, T. J., Rast, S., Redler, R., Reick, C. H., Rohrschneider, T., Schemann, V., Schmidt, H., Schnur, R., Schulzweida, U., Six, K. D., Stein, L., Stemmler, I., Stevens, B., von Storch, J.-S., Tian, F., Voigt, A., Vrese, P., Wieners, K.-H., Wilkenskjeld, S., Winkler, A., and Roeckner, E.: Developments in the MPI-M Earth System Model version 1.2 (MPI-ESM1.2) and Its Response to Increasing CO2, Journal of Advances in Modeling Earth Systems, 11, 998–1038, https://doi.org/10.1029/2018MS001400, 2019.

Maxwell, R. M. and Condon, L. E.: Connections between groundwater flow and transpiration partitioning, Science, 353, 377–380, https://doi.org/10.1126/science.aaf7891, 2016.

Meyer, H., Reudenbach, C., Wöllauer, S., and Nauss, T.: Importance of spatial predictor variable selection in machine learning applications – Moving from data reproduction to spatial prediction, Ecological Modelling, 411, 108 815, https://doi.org/10.1016/j.ecolmodel.2019.108815, 2019.

Milly, P. C. D. and Dunne, K. A.: Potential evapotranspiration and continental drying, Nature Climate Change, 6, 946–949, https://doi.org/10.1038/nclimate3046, 2016.

Milly, P. C. D. and Dunne, K. A.: Colorado River flow dwindles as warming-driven loss of reflective snow energizes evaporation, Science, 367, 1252–1255, https://doi.org/10.1126/science.aay9187, 2020.

Milly, P. C. D., Dunne, K. A., and Vecchia, A. V.: Global pattern of trends in streamflow and water availability in a changing climate, Nature, 438, 347–350, https://doi.org/10.1038/nature04312, 2005.

Miralles, D. G., Holmes, T. R. H., De Jeu, R. a. M., Gash, J. H., Meesters, A. G. C. A., and Dolman, A. J.: Global land-surface evaporation estimated from satellite-based observations, Hydrology and Earth System Sciences, 15, 453–469, https://doi.org/10.5194/hess-15-453-2011, 2011.

Muñoz-Sabater, J., Dutra, E., Agustí-Panareda, A., Albergel, C., Arduini, G., Balsamo, G., Boussetta, S., Choulga, M., Harrigan, S., Hersbach, H., Martens, B., Miralles, D. G., Piles, M., Rodríguez-Fernández, N. J., Zsoter, E., Buontempo, C., and Thépaut, J.-N.: ERA5-Land: a state-of-the-art global reanalysis dataset for land applications, Earth System Science Data, 13, 4349–4383, https://doi.org/10.5194/essd-13-4349-2021, 2021.

Nijssen, B., O'Donnell, G. M., Hamlet, A. F., and Lettenmaier, D. P.: Hydrologic Sensitivity of Global Rivers to Climate Change, Climatic Change, 50, 143–175, https://doi.org/10.1023/A:1010616428763, 2001.

Niu, G.-Y., Yang, Z.-L., Dickinson, R. E., and Gulden, L. E.: A simple TOPMODEL-based runoff parameterization (SIMTOP) for use in global climate models, Journal of Geophysical Research: Atmospheres, 110, https://doi.org/10.1029/2005JD006111, 2005.

Orth, R. and Destouni, G.: Drought reduces blue-water fluxes more strongly than green-water fluxes in Europe, Nature Communications, 9, 3602, https://doi.org/10.1038/s41467-018-06013-7, 2018.

Padrón, R. S., Gudmundsson, L., Liu, L., Humphrey, V., and Seneviratne, S. I.: Drivers of intermodel uncertainty in land carbon sink projections, Biogeosciences, 19, 5435–5448, https://doi.org/10.5194/bg-19-5435-2022, 2022.

Porkka, M., Virkki, V., Wang-Erlandsson, L., Gerten, D., Gleeson, T., Mohan, C., Fetzer, I., Jaramillo, F., Staal, A., te Wierik, S., Tobian, A., van der Ent, R., Döll, P., Flörke, M., Gosling, S. N., Hanasaki, N., Satoh, Y., Müller Schmied, H., Wanders, N., Famiglietti, J. S., Rockström, J., and Kummu, M.: Notable shifts beyond pre-industrial streamflow and soil moisture conditions transgress the planetary boundary for freshwater change, Nature Water, 2, 262–273, https://doi.org/10.1038/s44221-024-00208-7, 2024.

Riahi, K., Van Vuuren, D. P., Kriegler, E., Edmonds, J., O'Neill, B. C., Fujimori, S., Bauer, N., Calvin, K., Dellink, R., Fricko, O., Lutz, W., Popp, A., Cuaresma, J. C., Kc, S., Leimbach, M., Jiang, L., Kram, T., Rao, S., Emmerling, J., Ebi, K., Hasegawa, T., Havlik, P., Humpenöder, F., Da Silva, L. A., Smith, S., Stehfest, E., Bosetti, V., Eom, J., Gernaat, D., Masui, T., Rogelj, J., Strefler, J., Drouet, L., Krey, V., Luderer, G., Harmsen, M., Takahashi, K., Baumstark, L., Doelman, J. C., Kainuma, M., Klimont, Z., Marangoni, G., Lotze-Campen, H., Obersteiner, M., Tabeau, A., and Tavoni, M.: The Shared Socioeconomic Pathways and their energy, land use, and greenhouse gas emissions implications: An overview, Global Environmental Change, 42, 153–168, https://doi.org/10.1016/j.gloenvcha.2016.05.009, 2017.

Richardson, K., Steffen, W., Lucht, W., Bendtsen, J., Cornell, S. E., Donges, J. F., Drüke, M., Fetzer, I., Bala, G., von Bloh, W., Feulner, G., Fiedler, S., Gerten, D., Gleeson, T., Hofmann, M., Huiskamp, W., Kummu, M., Mohan, C., Nogués-Bravo, D., Petri, S., Porkka, M., Rahmstorf, S., Schaphoff, S., Thonicke, K., Tobian, A., Virkki, V., Wang-Erlandsson, L., Weber, L., and Rockström, J.: Earth beyond six of nine planetary boundaries, Science Advances, 9, eadh2458, https://doi.org/10.1126/sciadv.adh2458, 2023.

Rockström, J. and Gordon, L.: Assessment of green water flows to sustain major biomes of the world: Implications for future ecohydrological landscape management, Physics and Chemistry of the Earth, Part B: Hydrology, Oceans and Atmosphere, 26, 843–851, https://doi.org/10.1016/S1464-1909(01)00096-X, 2001.

Rockström, J., Donges, J. F., Fetzer, I., Martin, M. A., Wang-Erlandsson, L., and Richardson, K.: Planetary Boundaries guide humanity's future on Earth, Nature Reviews Earth & Environment, 5, 773–788, https://doi.org/10.1038/s43017-024-00597-z, 2024.

Ruehr, S., Keenan, T. F., Williams, C., Zhou, Y., Lu, X., Bastos, A., Canadell, J. G., Prentice, I. C., Sitch, S., and Terrer, C.: Evidence and attribution of the enhanced land carbon sink, Nature Reviews Earth & Environment, 4, 518–534, https://doi.org/10.1038/s43017-023-00456-3, 2023.

Scheff, J., Coats, S., and Laguë, M. M.: Why do the Global Warming Responses of Land-Surface Models and Climatic Dryness Metrics Disagree?, Earth's Future, 10, e2022EF002 814, 2022.

Schneider, U., Hänsel, S., Finger, P., Rustemeier, E., and Ziese, M.: GPCC Full Data Monthly Product Version 2022 at 1.0°: Monthly Land-Surface Precipitation from Rain-Gauges built on GTS-based and Historical Data, Deutscher Wetterdienst, https://doi.org/10.5676/DWD_GPCC/CLIM_M_V2022_100, 2022.

Seland, O., Bentsen, M., Olivié, D., Toniazzo, T., Gjermundsen, A., Graff, L. S., Debernard, J. B., Gupta, A. K., He, Y.-C., Kirkevåg, A., Schwinger, J., Tjiputra, J., Aas, K. S., Bethke, I., Fan, Y., Griesfeller, J., Grini, A., Guo, C., Ilicak, M., Karset, I. H. H., Landgren, O., Liakka, J., Moseid, K. O., Nummelin, A., Spensberger, C., Tang, H., Zhang, Z., Heinze, C., Iversen, T., and Schulz, M.: Overview of the Norwegian Earth System Model (NorESM2) and key climate response of CMIP6 DECK, historical, and scenario simulations, Geoscientific Model Development, 13, 6165–6200, https://doi.org/10.5194/gmd-13-6165-2020, 2020.

Sellar, A. A., Jones, C. G., Mulcahy, J. P., Tang, Y., Yool, A., Wiltshire, A., O'Connor, F. M., Stringer, M., Hill, R., Palmieri, J., Woodward, S., de Mora, L., Kuhlbrodt, T., Rumbold, S. T., Kelley, D. I., Ellis, R., Johnson, C. E., Walton, J., Abraham, N. L., Andrews, M. B., Andrews, T., Archibald, A. T., Berthou, S., Burke, E., Blockley, E., Carslaw, K., Dalvi, M., Edwards, J., Folberth, G. A., Gedney, N., Griffiths, P. T., Harper, A. B., Hendry, M. A., Hewitt, A. J., Johnson, B., Jones, A., Jones, C. D., Keeble, J., Liddicoat, S., Morgenstern, O., Parker, R. J., Predoi, V., Robertson, E., Siahaan, A., Smith, R. S., Swaminathan, R., Woodhouse, M. T., Zeng, G., and Zerroukat, M.:

UKESM1: Description and Evaluation of the U.K. Earth System Model, Journal of Advances in Modeling Earth Systems, 11, 4513–4558, https://doi.org/10.1029/2019MS001739, 2019.

Seneviratne, S. I., Corti, T., Davin, E. L., Hirschi, M., Jaeger, E. B., Lehner, I., Orlowsky, B., and Teuling, A. J.: Investigating soil moisture–climate interactions in a changing climate: A review, Earth-Science Reviews, 99, 125–161, https://doi.org/10.1016/j.earscirev.2010.02.004, 2010.

Singh, N. K., Emanuel, R. E., McGlynn, B. L., and Miniat, C. F.: Soil Moisture Responses to Rainfall: Implications for Runoff Generation, Water Resources Research, 57, e2020WR028 827, https://doi.org/10.1029/2020WR028827, _eprint: https://agupubs.onlinelibrary.wiley.com/doi/pdf/10.1029/2020WR028827, 2021.

Skinner, C. B., Poulsen, C. J., Chadwick, R., Diffenbaugh, N. S., and Fiorella, R. P.: The Role of Plant CO2 Physiological Forcing in Shaping Future Daily-Scale Precipitation, Journal of Climate, 30, 2319–2340, https://doi.org/10.1175/JCLI-D-16-0603.1, 2017.

Spracklen, D. V., Arnold, S. R., and Taylor, C. M.: Observations of increased tropical rainfall preceded by air passage over forests, Nature, 489, 282–285, https://doi.org/10.1038/nature11390, 2012.

Stein, L., Mukkavilli, S. K., Pfitzmann, B. M., Staar, P. W. J., Ozturk, U., Berrospi, C., Brunschwiler, T., and Wagener, T.: Wealth Over Woe: Global Biases in Hydro-Hazard Research, Earth's Future, 12, e2024EF004 590, https://doi.org/10.1029/2024EF004590, 2024.

Stigter, E. E., Litt, M., Steiner, J. F., Bonekamp, P. N. J., Shea, J. M., Bierkens, M. F. P., and Immerzeel, W. W.: The Importance of Snow Sublimation on a Himalayan Glacier, Frontiers in Earth Science, 6, https://doi.org/10.3389/feart.2018.00108, 2018.

Swann, A. L. S., Hoffman, F. M., Koven, C. D., and Randerson, J. T.: Plant responses to increasing CO2 reduce estimates of climate impacts on drought severity, Proceedings of the National Academy of Sciences, 113, 10 019–10 024, https://doi.org/10.1073/pnas.1604581113, 2016.

Swart, N. C., Cole, J. N. S., Kharin, V. V., Lazare, M., Scinocca, J. F., Gillett, N. P., Anstey, J., Arora, V., Christian, J. R., Hanna, S., Jiao, Y., Lee, W. G., Majaess, F., Saenko, O. A., Seiler, C., Seinen, C., Shao, A., Sigmond, M., Solheim, L., von Salzen, K., Yang, D., and Winter, B.: The Canadian Earth System Model version 5 (CanESM5.0.3), Geoscientific Model Development, 12, 4823–4873, https://doi.org/10.5194/gmd-12-4823-2019, 2019.

Séférian, R., Nabat, P., Michou, M., Saint-Martin, D., Voldoire, A., Colin, J., Decharme, B., Delire, C., Berthet, S., Chevallier, M., Sénési, S., Franchisteguy, L., Vial, J., Mallet, M., Joetzjer, E., Geoffroy, O., Guérémy, J.-F., Moine, M.-P., Msadek, R., Ribes, A., Rocher, M., Roehrig, R., Salas-y Mélia, D., Sanchez, E., Terray, L., Valcke, S., Waldman, R., Aumont, O., Bopp, L., Deshayes, J., Éthé, C., and Madec, G.: Evaluation of CNRM Earth System Model, CNRM-ESM2-1: Role of Earth System Processes in Present-Day and Future Climate, Journal of Advances in Modeling Earth Systems, 11, 4182–4227, https://doi.org/10.1029/2019MS001791, 2019.

Tabari, H.: Climate change impact on flood and extreme precipitation increases with water availability, Scientific Reports, 10, 13 768, https://doi.org/10.1038/s41598-020-70816-2, 2020.

Trenberth, K. E.: Conceptual Framework for Changes of Extremes of the Hydrological Cycle with Climate Change, Climatic Change, 42, 327–339, https://doi.org/10.1023/A:1005488920935, 1999.

Trenberth, K. E.: Changes in precipitation with climate change, Climate Research, 47, 123–138, https://doi.org/10.3354/cr00953, 2011.

Ukkola, A. M., Prentice, I. C., Keenan, T. F., van Dijk, A. I. J. M., Viney, N. R., Myneni, R. B., and Bi, J.: Reduced streamflow in water-stressed climates consistent with CO2 effects on vegetation, Nature Climate Change, 6, 75–78, https://doi.org/10.1038/nclimate2831, 2016.

Wada, Y., van Beek, L. P. H., and Bierkens, M. F. P.: Modelling global water stress of the recent past: on the relative importance of trends in water demand and climate variability, Hydrology and Earth System Sciences, 15, 3785–3808, https://doi.org/10.5194/hess-15-3785-2011, 2011.

Wada, Y., Flörke, M., Hanasaki, N., Eisner, S., Fischer, G., Tramberend, S., Satoh, Y., van Vliet, M. T. H., Yillia, P., Ringler, C., Burek, P., and Wiberg, D.: Modeling global water use for the 21st century: the Water Futures and Solutions (WFaS) initiative and its approaches, Geoscientific Model Development, 9, 175–222, https://doi.org/10.5194/gmd-9-175-2016, 2016.

Wada, Y., Bierkens, M. F. P., de Roo, A., Dirmeyer, P. A., Famiglietti, J. S., Hanasaki, N., Konar, M., Liu, J., Müller Schmied, H., Oki, T., Pokhrel, Y., Sivapalan, M., Troy, T. J., van Dijk, A. I. J. M., van Emmerik, T., Van Huijgevoort, M. H. J., Van Lanen, H. A. J., Vörösmarty, C. J., Wanders, N., and Wheater, H.: Human–water interface in hydrological modelling: current status and future directions, Hydrology and Earth System Sciences, 21, 4169–4193, https://hess.copernicus.org/articles/21/4169/2017/, 2017.

Wagener, T., Reinecke, R., and Pianosi, F.: On the evaluation of climate change impact models, WIREs Climate Change, 13, e772, https://doi.org/10.1002/wcc.772, 2022.

Wang, Y., Hu, J., Li, R., Song, B., Hailemariam, M., Fu, Y., and Duan, J.: Increasing Cloud Coverage Deteriorates Evapotranspiration Estimating Accuracy From Satellite, Reanalysis and Land Surface Models Over East Asia, Geophysical Research Letters, 50, e2022GL102 706, https://doi.org/10.1029/2022GL102706, 2023.

Wang-Erlandsson, L., Tobian, A., van der Ent, R. J., Fetzer, I., te Wierik, S., Porkka, M., Staal, A., Jaramillo, F., Dahlmann, H., Singh, C., Greve, P., Gerten, D., Keys, P. W., Gleeson, T., Cornell, S. E., Steffen, W., Bai, X., and Rockström, J.: A planetary boundary for green water, Nature Reviews Earth & Environment, 3, 380–392, https://doi.org/10.1038/s43017-022-00287-8, 2022.

Wei, H., Zhang, Y., Huang, Q., Chiew, F. H. S., Luan, J., Xia, J., and Liu, C.: Direct vegetation response to recent CO2 rise shows limited effect on global streamflow, Nature Communications, 15, 9423, https://doi.org/10.1038/s41467-024-53879-x, 2024.

Wei, H., Zhang, Y., Huang, Q., Liu, C., and Wagener, T.: Functional Relationships Reveal Large Differences in Streamflow Response to eCO2-Vegetation in Global Water Models, Geophysical Research Letters, 52, e2024GL113 685, https://doi.org/10.1029/2024GL113685, 2025.

Weiskel, P. K., Wolock, D. M., Zarriello, P. J., Vogel, R. M., Levin, S. B., and Lent, R. M.: Hydroclimatic regimes: a distributed water-balance framework for hydrologic assessment, classification, and management, Hydrology and Earth System Sciences, 18, 3855–3872, https://doi.org/10.5194/hess-18-3855-2014, 2014.

Wu, R.-J., Lo, M.-H., and Scanlon, B. R.: The Annual Cycle of Terrestrial Water Storage Anomalies in CMIP6 Models Evaluated against GRACE Data, Journal of Climate, 34, 8205–8217, https://doi.org/10.1175/JCLI-D-21-0021.1, 2021.

Wu, T., Lu, Y., Fang, Y., Xin, X., Li, L., Li, W., Jie, W., Zhang, J., Liu, Y., Zhang, L., Zhang, F., Zhang, Y., Wu, F., Li, J., Chu, M., Wang, Z., Shi, X., Liu, X., Wei, M., Huang, A., Zhang, Y., and Liu, X.: The Beijing Climate Center Climate System Model (BCC-CSM): the main progress from CMIP5 to CMIP6, Geoscientific Model Development, 12, 1573–1600, https://doi.org/10.5194/gmd-12-1573-2019, 2019.

Yang, H., Piao, S., Huntingford, C., Ciais, P., Li, Y., Wang, T., Peng, S., Yang, Y., Yang, D., and Chang, J.: Changing the retention properties of catchments and their influence on runoff under climate change, Environmental Research Letters, 13, 094 019, https://doi.org/10.1088/1748-9326/aadd32, 2018.

Yang, Y., McVicar, T. R., Yang, D., Zhang, Y., Piao, S., Peng, S., and Beck, H. E.: Low and contrasting impacts of vegetation CO_2 fertilization on global terrestrial runoff over 1982–2010: accounting for aboveground and belowground vegetation–CO_2 effects, Hydrology and Earth System Sciences, 25, 3411–3427, https://doi.org/10.5194/hess-25-3411-2021, 2021.

Yang, Y., Roderick, M. L., Guo, H., Miralles, D. G., Zhang, L., Fatichi, S., Luo, X., Zhang, Y., McVicar, T. R., Tu, Z., Keenan, T. F., Fisher, J. B., Gan, R., Zhang, X., Piao, S., Zhang, B., and Yang, D.: Evapotranspiration on a greening Earth, Nature Reviews Earth & Environment, 4, 626–641, https://doi.org/10.1038/s43017-023-00464-3, 2023.

Yin, J., Gentine, P., Zhou, S., Sullivan, S. C., Wang, R., Zhang, Y., and Guo, S.: Large increase in global storm runoff extremes driven by climate and anthropogenic changes, Nature Communications, 9, 4389, https://doi.org/10.1038/s41467-018-06765-2, 2018.

Young, A. M., Friedl, M. A., Novick, K., Scott, R. L., Moon, M., Frolking, S., Li, X., Carrillo, C. M., and Richardson, A. D.: Disentangling the Relative Drivers of Seasonal Evapotranspiration Across a Continental-Scale Aridity Gradient, Journal of Geophysical Research: Biogeosciences, 127, e2022JG006 916, https://doi.org/10.1029/2022JG006916, _eprint: https://agupubs.onlinelibrary.wiley.com/doi/pdf/10.1029/2022JG006916, 2022.

Zaitchik, B. F., Rodell, M., Biasutti, M., and Seneviratne, S. I.: Wetting and drying trends under climate change, Nature Water, 1, 502–513, https://doi.org/10.1038/s44221-023-00073-w, 2023.

Zhao, Q., Zhu, Z., Zeng, H., Zhao, W., and Myneni, R. B.: Future greening of the Earth may not be as large as previously predicted, Agricultural and Forest Meteorology, 292-293, 108 111, https://doi.org/10.1016/j.agrformet.2020.108111, 2020.

Zheng, H., Yang, Z.-L., Lin, P., Wei, J., Wu, W.-Y., Li, L., Zhao, L., and Wang, S.: On the Sensitivity of the Precipitation Partitioning Into Evapotranspiration and Runoff in Land Surface Parameterizations, Water Resources Research, 55, 95–111, https://doi.org/10.1029/2017WR022236, 2019.

Zhu, Z., Piao, S., Myneni, R. B., Huang, M., Zeng, Z., Canadell, J. G., Ciais, P., Sitch, S., Friedlingstein, P., Arneth, A., Cao, C., Cheng, L., Kato, E., Koven, C., Li, Y., Lian, X., Liu, Y., Liu, R., Mao, J., Pan, Y., Peng, S., Peñuelas, J., Poulter, B., Pugh, T. A. M., Stocker, B. D., Viovy, N., Wang, X., Wang, Y., Xiao, Z., Yang, H., Zaehle, S., and Zeng, N.: Greening of the Earth and its drivers, Nature Climate Change, 6, 791–795, https://doi.org/10.1038/nclimate3004, 2016.